

Ch/nHA/ZnO Coated Surgical Staple Pins for Enhanced Corrosion Resistance and Antibacterial Performance



By

Romana Afsheen

School of Chemical and Material Engineering

National University of Science and Technology

2024

Ch/nHA/ZnO Coated Surgical Staple Pins for Enhanced Corrosion Resistance and Antibacterial Performance



Name: Romana Afsheen

Registration. No.: Fall-2020-MS-MSE-15-00000327769

**This thesis is submitted as a partial fulfillment of the requirements for the
degree of**

MS in Materials and Surface Engineering

Supervisor Name: Dr. Muhammad Shoaib Butt

School of Chemical and Materials Engineering (SCME)

National University of Sciences and Technology (NUST)

H-12 Islamabad, Pakistan

January, 2024



THESIS ACCEPTANCE CERTIFICATE

Certified that final copy of MS thesis written by Ms **Romana Afsheen** (Registration No 00000327769), of School of Chemical & Materials Engineering (SCME) has been vetted by undersigned, found complete in all respects as per NUST Statues/Regulations, is free of plagiarism, errors, and mistakes and is accepted as partial fulfillment for award of MS degree. It is further certified that necessary amendments as pointed out by GEC members of the scholar have also been incorporated in the said thesis.

Signature: _____

Name of Supervisor: Dr M. Shoaib Butt

Date: 18th Jan, 2024

7. Signature (HOD): _____

Date: 24.1.2024

Signature (Dean/Principal): _____

Date: 24.1.2024



Form TH-1
(Must be type written)

National University of Sciences & Technology (NUST)

MASTER'S THESIS WORK

Formulation of Guidance and Examination Committee (GEC)

Name: Romana Afsheen NUST Regn No: 327769
 Department: SCME, MSE-15 Specialization: Materials and surface Engineering
 Credit Hour Completed: 21/24 CGPA: 3.93/3.94

Course Work Completed

S/No	Code	Title	Core/Elective	CH	Grade
1	MSE-821	Mechanical Behavior of Materials	Core	3	A
2	MSE-811	Materials Thermodynamics	Core	3	B+
3	MSE-881	Manufacturing processes	Elective	3	A
4	RM-898	Research Methodology	Additional	2	Q
5	MSE-812	Phase Transformation and microstructures	Core	3	A
6	MSE-851	Surface Engineering and Characterization	Core	3	A
7	MSE-872	Composite Materials	Elective	3	A
8	MSE-861	Engineering Ceramics and Glasses	Elective	3	A

Date: 29/09/2021
 Student's Signature: Romana Afsheen
 Title: MSE-854 Characterization of materials

Thesis Committee

- Name: Dr. Muhammad Shoaib But (Supervisor) Signature: [Signature]
- Name: Dr. Shahrukh Abbas (Co-Supervisor) (External) Signature: [Signature]
Department: ASAB
- Name: Dr. Adeel Signature: [Signature]
Department: SCME
- Name: Dr. Aftab Akram Signature: [Signature]
Department: SCME

Date: 25/10/2021
 Signature of Head of Department: [Signature]

APPROVAL

Date: 25-10-2021
 Dean/Principal: [Signature]

Distribution

- 1x copy to Exam Branch, Main Office NUST
- 1x copy to PGP Dte, Main Office NUST
- 1x copy to Exam branch, respective Institute.

School of Chemical and Materials Engineering (SCME) Sector H-12, Islamabad



National University of Sciences & Technology (NUST)

FORM TH-4

MASTER'S THESIS WORK

We hereby recommend that the dissertation prepared under our supervision by
Regn No & Name: 00000327769 Romana Afsheen

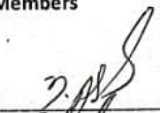
Title: Ch/nHA/ZnO coated Surgical Staple Pins for Enhanced Corrosion Resistance and Antibacterial Performance.

Presented on: 18 Jan 2024 at: 1400 hrs in SCME (Seminar Hall)

Be accepted in partial fulfillment of the requirements for the award of Masters of Science degree in
Materials & Surface Engineering.

Guidance & Examination Committee Members

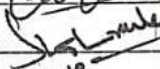
Name: Dr Muhammad Aftab Akram

Signature: 

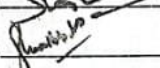
Name: Dr Malik Adeel Umer

Signature: 

Name: Dr Shahrukh Abbas (Co-Supervisor -ASAB)

Signature: 

Supervisor's Name: Dr Muhammad Shoaib Butt

Signature: 

Dated: 18th Jan, 2023


Head of Department
Date 22/1/24


Dean/Principal
Date 22-1-2024

School of Chemical & Materials Engineering (SCME)

Dedication

"To my Grand Father, who is no longer with me to witness me complete my work. May I have the same unwavering dedication to my field in science that you had in me."

Acknowledgments

All admiration to Allah Almighty. He is the One, who bestows and gives us the power to us to think, utilize our expertise in knowledge in achieving remarkable solutions for mankind in every field. Therefore, I express my greatest thanks to Almighty Allah the universal and the architect of the world. Allah Almighty says in Quran: “Read! In the name of your lord” (Alaq; 1st revealed ayah). This Quranic verse beautifully encapsulates the profound significance of education in the lives of human beings.

I want to convey my sincere thanks to my esteemed and kind supervisor, **Dr. Muhammad Shoaib Butt**, and my co-supervisor, **Dr. Shahrukh Abbas** from ASAB, NUST, for their unwavering guidance and patience, which steered me towards the successful completion of my project and thesis. Their composed and encouraging behavior served as a constant source of motivation for me, bringing out the best in my efforts. Their invaluable suggestions and constructive feedback greatly enriched the content of this thesis. I extend my deepest gratitude to my teachers for their guidance and motivation in enabling me to perform at my best. Additionally, I would like to express appreciation to my parents, family members, and friends for their assistance, prayers, and valuable advice.

I want to thank my GEC member, **Dr. Muhamamd Aftab Akram** and **Dr. Malik Adeel Umer** for their continuous support and motivation which helped me at various stages during my Masters. I also want to thank **Dr. Fazal Adnan** from ASAB, NUST for his support as he helped a lot during characterization and lab work.

I would like to thank each member who helped me a lot during my research and kept me motivated throughout this journey. I acknowledge the support provided by the Materials Engineering department of SCME for providing me with a platform to perform my experiments and using my skills in research work. Lastly, I want to thank my family for their support and prayers.

Romana Afsheen

Abstract

Surgical Staple Pins (SSPs) play a significant role during the wound healing of surgical site infection in the medical world. This project focuses on enhancing the biocompatibility and performance of surgical staples through the synthesis of a specialized coating. Surgical staples are widely used in various medical procedures for wound closure and tissue approximation, offering advantages such as speed, consistency, minimal tissue reaction, and reduced scarring. However, to further improve their effectiveness, we aimed to develop a coating with specific properties. The selected materials for the coating include chitosan (matrix) i.e., biocompatible, and biodegradable polymer, nanohydroxyapatite (nHA), and zinc oxide nanoparticles (ZnO) (fillers). Chitosan's properties make it suitable for wound healing applications, with antibacterial, analgesic, and hemostatic qualities. Bioactive glasses and nHA promote soft tissue regeneration and are known to expedite skin regeneration by encouraging angiogenesis and collagen deposition during the wound healing process. ZnO nanoparticles provide antibacterial properties and can enhance corrosion resistance. The incorporation of these materials into the coating aims to create a surface that is biocompatible, antibacterial, and conducive to wound healing. It must have good or improved corrosion resistance. This coating process has the potential to reduce the risk of tissue irritation, inflammation, and infections while promoting faster and more efficient healing. Therefore the composite was prepared and was coated through Electrophoretic deposition Method on SSPs. The treated / coated SSPs were then evaluated and compared, with non-treated / uncoated SSPS acting as the control. The corrosion resistance samples were carried out using Hank's solution having pH of approximately 6.8. The corrosion resistance properties were improved having the lower values of I_{corr} of the treated SSPs with Ch /nHA /ZnO Composite films as compared to the untreated and SSPs. The antibacterial activity of these samples was also observed against bacterial strains of Escherichia coli and Staphylococcus aureus. In vitro antibacterial tests of these coated SSPs were carried out. The Ch/ nHA /ZnO coated SSPs showed promising antibacterial activity. Through this study, it was found that the Surgical Staple Pins coated with Ch /nHA /ZnO Composite films have improved corrosion resistance and antibacterial properties, and they have the potential to be used for wound healing.

Table of Contents

Dedication	I
Acknowledgments	II
Abstract.....	III
Chapter 1:.....	1
Introduction.....	1
1.1 Biomedical science.....	1
1.1.1 Types of Biomedical Science.....	2
1.2 Biomedical Applications	3
1.3 Wounds.....	4
1.4 Wound Healing.....	5
1.5 Stages of Wound Healing	5
1.5.1 Hemostasis	5
1.5.2 Inflammation.....	5
1.5.3 Proliferation	5
1.5.4 Remodeling (Maturation).....	6
1.6 History of Treating Wounds	7
1.7 Surgical Sutures and Types	8
1.8 Surgical staples	8

1.9	Aims of the Project	9
Chapter 2:		10
Literature Review		10
2.1	Surgical staples	10
2.2	Selection of materials	14
2.2.1	Chitosan	15
2.2.2	Bioactive Glasses (BG) / Nanohydroxyapatite (nHA).....	16
2.2.3	Zinc Oxide Nanoparticles (ZnO)	19
Chapter 3:		21
Materials and Methods.....		21
3.1	Synthesis route:	21
3.1.1	Wet- chemical synthesis	21
3.2	Methods for coatings	22
3.2.1	Electrodeposition Coating	22
3.2.1.1	Electrolytic deposition	23
3.2.1.2	Electrophoretic deposition	23
3.3	Aims and Objectives	24
3.4	Synthesis of ZnO Nanoparticles:	24
3.5	Synthesis of Hydroxyapatite Nanoparticles (nHA).....	25

3.6	Selected Coating Method	27
3.6.1	Suspension preparation.....	27
3.7	Electrophoretic deposition.....	28
Chapter 4:		29
Characterization Techniques		29
4.1	Scanning Electron Microscope (SEM).....	29
4.2	X-RAY Diffraction (XRD)	30
4.3	Fourier Transform Infrared Spectroscopy (FTIR)	30
4.4	Electrochemical Workstation	31
4.4.1	Corrosion testing.....	32
4.4.2	Hanks's Solution.....	32
4.5	Antimicrobial testing.....	33
4.5.1	Diffusion method.....	33
4.5.2	Dilution method.....	34
4.5.3	Colony Forming Unit (CFU)	34
Chapter 5:		36
Results and Discussion.....		36
5.1	X-Ray Diffraction	36
5.2	Fourier Transform Infrared Analysis	39

5.3	Scanning Electron Microscopy (SEM)	44
5.4	Electrochemical corrosion in Hank's Solution.....	49
5.5	Antimicrobial activity	53
5.5.1	Disc Diffusion Method	54
5.5.2	Colony Forming Unit (CFU)	55
Conclusion		59

List of Figures

Figure 1: Main Disciplines of Biomedical Sciences	2
Figure 2: Biomedical Applications	3
Figure 3: Wound Healing Steps	6
Figure 4: XRD of ZnO NPs	36
Figure 5: XRD of nHA.....	37
Figure 6: XRD of Chitosan	38
Figure 7: XRD of Ch/ nHA/ ZnO	39
Figure 8: FTIR of Chitosan.....	40
Figure 9: FTIR of ZnO.....	41
Figure 10: FTIR of nHA	42
Figure 11: FTIR of Ch/ nHA/ ZnO	43
Figure 12: SEM of Chitosan	44
Figure 13: SEM of ZnO NP	44
Figure 14: SEM of nHA.....	45
Figure 15: SEM of Ch/ nHA/ZnO	46
Figure 16: SEM of ZnO coated on SSP	46
Figure 17: SEM of nHA on SSP	47
Figure 18: SEM of Ch/ nHA/ ZnO coated on SSP	48

Figure 19: SEM of Ch/ nHA/ ZnO coated on SSP(closer view)	48
Figure 20: Corrosion Testing Results	51
Figure 21: Incubation zones for against E. coli and S. aureus.....	54

List of Tables

<i>Table 1: Comparison of the Corrosion Properties.....</i>	<i>51</i>
---	-----------

Chapter 1:

Introduction

1.1 Biomedical science

Biomedical science is a scientific discipline focused on understanding the intricacies of the human body at the molecular level. Its primary objective is to advance medical knowledge and discover novel treatments for various infections and diseases. Within the realm of biomedical sciences, research extends to the field of drug delivery methods for combating diverse infections. Additionally, clinical epidemiology falls under the umbrella of biomedical science, which encompasses healthcare and public health. The central mission of biomedical science is to safeguard human health.

In contemporary times, biomedical science has become an expansive field that plays a pivotal role in supporting modern medicine. It involves in-depth analyses of the human body in both its healthy and diseased states. A major emphasis of biomedical science is on studying diseases and their associated symptoms within the human body. Recent advancements in biomedical science have led to the development of highly effective antibacterial and anti-inflammatory medications, particularly in the context of wound healing applications. Modern medical techniques and treatments derived from biomedical science have proven immensely beneficial in managing a wide array of illnesses.

Microbiology is a fundamental component of biomedical science, involving the study of various microorganisms, including bacteria, fungi, and parasites, which have the potential to cause infections. By thoroughly investigating infections, biomedical scientists can identify appropriate interventions, such as the use of antibiotics or antibacterial drugs, to target and treat infections effectively at the source.

1.1.1 Types of Biomedical Science

Biomedical science is a broad and multidisciplinary field that encompasses several main disciplines or areas of study. These main disciplines within biomedical science include:



Figure 1: Main Disciplines of Biomedical Sciences

These main disciplines within biomedical science work together to advance our understanding of human health and disease, develop innovative medical treatments, and improve healthcare outcomes. They often overlap and collaborate to address complex biomedical challenges.

1.2 Biomedical Applications

Biomedical science boasts a wide array of applications, including the development of innovative drug delivery systems. One noteworthy approach involves incorporating anti-microbial or anti-inflammatory drugs into surgical sutures, which greatly enhances the wound healing process. This method harnesses the potent antimicrobial properties to combat diverse bacterial strains responsible for various infections.

Biomedical science spans a wide range of applications, from enhancing wound healing through drug delivery to enabling real-time observation of biological activities via bioimaging and facilitating the precise detection of target analytes using biosensors. These applications underscore the field's far-reaching impact on healthcare, diagnostics, and scientific research. Some key biomedical applications are shown in figure below:

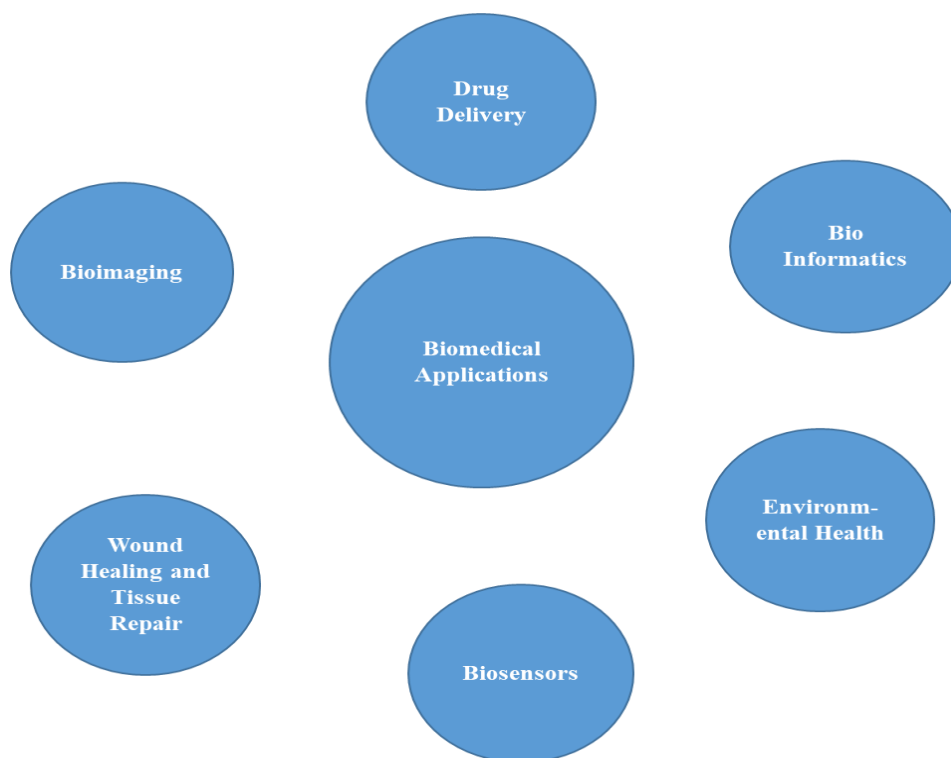


Figure 2: Biomedical Applications

1.3 Wounds

A "wound" is typically defined as a type of injury to the body's tissues, typically involving a break in the skin. It refers to injuries that cause damage to our body's cells and tissues. They can be classified in various ways based on the time it takes for them to heal. Broadly speaking, wounds are primarily categorized into two main types: open wounds and closed wounds.

Open wounds and closed wounds result from sudden actions, such as cuts, falls, or impacts. Examples of wounds include cuts, grazes, and lacerations. Cuts, for instance, are typically caused by sharp objects like knives, glass, or even very sharp and thin sheets of paper when they meet the human body.

Wounds can result from a variety of causes, including accidents, surgery, burns, or diseases. There are different types of wounds, such as:

In Open wound, the skin is broken, and the underlying tissues may be exposed. Examples include cuts, lacerations, and puncture wounds.

Close wounds do not involve a break in the skin, but they may still result in damage to the underlying tissues. Examples include contusions (bruises) and hematomas (localized collection of blood). Acute wounds are typically caused by a sudden injury and go through a predictable healing process. Chronic wounds are those that take longer to heal and are often associated with underlying health conditions, like diabetes or vascular disorders.

These are wounds created intentionally during surgery. They are typically closed with sutures, staples, or other methods to promote healing.

The treatment and management of wounds depend on their type, size, location, and the underlying health of the individual. Effective wound care is crucial to prevent infections and facilitate the healing process. It often involves cleaning the wound, applying appropriate dressings, and, in some cases, sutures or other medical interventions.

1.4 Wound Healing

Wound healing is the natural biological mechanism by which the body repairs and rejuvenates damaged or injured tissues after an injury or wound occurs. It is a complex and highly orchestrated series of events that aims to restore the structural and functional integrity of the affected tissue. The primary goal of wound healing is to close the wound, replace damaged tissue with healthy tissue, and ultimately restore normal function.

1.5 Stages of Wound Healing

It involves several stages, which can overlap and vary in duration depending on the type of them and how severe it is, as well as The general well-being of the individual [1, 2]. The typical stages of wound healing are:

1.5.1 Hemostasis

This is the initial stage that begins immediately after a wound occurs. It encompasses the inherent physiological reaction of the body to halt bleeding. Blood vessels constrict (vasoconstriction) to reduce blood flow, and platelets form clots to plug the wound (hemostasis). This temporary barrier helps prevent excessive blood loss.

1.5.2 Inflammation

After hemostasis, the body enters an inflammatory phase. Inflammation is a necessary response to injury as it helps remove debris and pathogens from the wound site. During this stage, white blood cells (neutrophils and macrophages) are recruited to the area to fight infection and begin cleaning the wound. Inflammation is often characterized by redness, swelling, heat, and pain.

1.5.3 Proliferation

This stage involves the rebuilding of damaged tissue. Fibroblasts, specialized cells, start producing collagen, a structural protein that forms the foundation for new tissue. New blood vessels also form in a process called angiogenesis, which provides oxygen and nutrients to

support tissue growth. Epithelial cells from the surrounding wound edges move to encase and close the wound.

1.5.4 Remodeling (Maturation)

The final stage of wound healing can last for months or even years. During this stage, the recently developed tissue undergoes remodeling and maturation. Collagen fibers are rearranged and strengthened, and the scar tissue becomes less prominent and more like the surrounding tissue. This stage aims to improve the wound's overall strength and functionality.

It's important to note that not all wounds heal perfectly, and factors such as age, overall health, and the presence of underlying medical conditions can affect the healing process. Some wounds may result in noticeable scars, while others may heal with minimal scarring. Proper wound care, including keeping the wound clean and protected, can help facilitate the healing process and reduce the risk of complications. In some cases, medical interventions such as sutures, staples, or wound dressings may be necessary to aid in wound closure and healing.

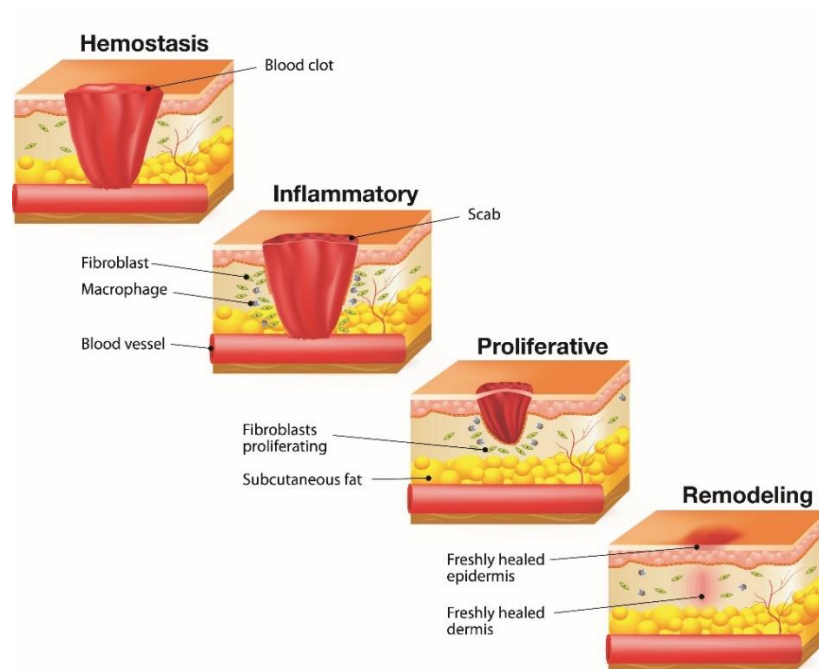


Figure 3: Wound Healing Steps

1.6 History of Treating Wounds

The history of treating wounds is a rich tapestry of human ingenuity, evolving from rudimentary practices to sophisticated medical techniques. In ancient civilizations, such as Egypt, Greece, and Rome, wound care often relied on natural substances like honey, which exhibited antibacterial properties, as well as wine and herbal concoctions. The application of these substances was based more on tradition and intuition rather than scientific understanding. While some of these practices had merit, they were limited in their effectiveness.

The turning point in wound care came in the late 19th century with the groundbreaking discoveries of germ theory and antiseptic principles. Louis Pasteur's germ theory established the link between microorganisms and infections, fundamentally altering our perception of wound management. Joseph Lister, a British surgeon, further revolutionized the field by introducing the use of carbolic acid (phenol) as an antiseptic during surgeries. This marked the beginning of sterile surgical techniques, drastically reducing the risk of infection during procedures [3, 4].

As the 20th century dawned, wound care saw remarkable advancements. The discovery and widespread use of antibiotics, most notably penicillin, transformed infection control. Now, physicians can treat bacterial infections that had previously been lethal. Sterile gauze and adhesive bandages also became fundamental tools in wound dressings, offering protection while facilitating the healing process [5].

Surgical techniques for wound closure continued to evolve. Stitches, or sutures, became a cornerstone of wound closure. These sutures, made from various materials such as silk, nylon, or absorbable materials, allowed healthcare providers to meticulously bring together wound edges for optimal healing. Sutures have remained a mainstay in wound closure for decades, employed in a wide range of surgical procedures and wound management scenarios [6].

However, in recent decades, alternative methods for wound closure have gained prominence. One notable advancement is the use of staples. Surgical staplers are used in specific situations, such as large incisions or deep wounds, where suturing might be more challenging. Staples

offer several advantages, including speed, precision, and reduced tissue trauma. They are particularly useful in surgical settings and can be a valuable alternative to traditional sutures.

1.7 Surgical Sutures and Types

Surgical stitches, also known as sutures, are a crucial part of wound closure in medical procedures. They are used to bring together the edges of a wound or incision to facilitate healing and minimize scarring. Surgical sutures are at risk of bacterial infections and the development of biofilms [7]. Furthermore, the presence of sutures can lead to pain and unwanted, excessive inflammation at the wound site, which can hinder the healing process [8].

There are various types of surgical sutures, each designed for specific applications based on factors like the location of the wound, the tissue being sutured, and the desired outcome. Some common types of surgical stitches include absorbable sutures and non- absorbable sutures.

Absorbable sutures are designed to break down and be absorbed by the body over time. They are typically used for internal tissues that don't require long-term support.

Non- absorbable sutures are designed to remain in the body indefinitely and may require removal once the wound has healed.

In some cases, tissue adhesives (glues) or staples may be used instead of traditional sutures, especially for superficial wounds or in situations where suturing may be impractical.

1.8 Surgical staples

The focus of our project is the surgical staples. Surgical staples are medical devices commonly used in various surgical procedures for wound closure and tissue approximation. They offer a quick and efficient means of closing incisions and are particularly useful in situations where sutures may be impractical or time-consuming. These devices are commonly utilized as alternatives to traditional sutures. They offer several advantages, including the ability to efficiently seal sizable wounds or incisions with reduced discomfort for patients compared to stitches. These devices are frequently employed in minimally invasive surgical procedures [9].

Additionally, they are beneficial for suturing wounds in regions where the skin closely adheres to bone, as well as in surgeries involving the removal of organs or the reconnection of various internal organ parts.

1.9 Aims of the Project

The aim of the project is to synthesize a composite material which should be biocompatible, have anti-bacterial properties, help in skin regeneration, and thereby accelerate the wound healing process. This synthesized material is then coated over the surgical staple pins to enhance their performance and biocompatibility through a specific coating process, thereby improving the corrosion resistance and antibacterial properties of the surgical staple pins.

These coatings serve several important purposes. Firstly, they reduce the risk of tissue irritation and inflammation by providing a smooth and biocompatible surface that minimizes friction against the surrounding tissues. Secondly, some coatings are antibacterial, helping to prevent infections at the site of staple placement.

These coatings play a crucial role in ensuring the safety and effectiveness of surgical staple pins in a wide range of medical procedures.

Chapter 2:

Literature Review

Wound closure is a common surgical practice, with over 80% of procedures utilizing various methods. The choice of technique depends on factors such as wound type, location, patient age, and tissue characteristics. Surgical sutures, the most widely used method, have limitations, including dehiscence and scarring. They also require skilled personnel, risking poor blood supply and bacterial colonization [10].

2.1 Surgical staples

Surgical staples have gained attention due to their efficiency, mechanical strength, and low infection risk, especially during the COVID-19 pandemic. Although no ideal staple has been developed to address all complications, they offer an appealing alternative [11].

Surgical staples are the medical devices used to deal with deep wounds that require stitching. The use of staples for intestinal anastomosis is a widely adopted and common practice in modern surgery [12-14].

Surgical staplers are commonly employed in medical procedures to secure incisions in the abdomen and uterus, particularly in the context of Cesarean deliveries (C-sections). Their use in these cases facilitates faster healing and reduces the formation of excessive scar tissue. Surgeons also turn to surgical staplers when they must excise a segment of an organ or create incisions through diverse organs and tissues within the body [15].

These devices are crucial for connecting or reconnecting internal organs within a specific organ system. Surgeons commonly employ surgical staplers in procedures related to the digestive tract, including the esophagus, stomach, and intestines. During these procedures, a portion of

these structures may undergo removal, necessitating the reconnection of the remaining sections using surgical staples.

Surgical staplers operate by compressing tissue, joining two pieces of tissue with staggered rows of B-shaped surgical staples, and, in certain models, excising excess tissue to achieve a tidy closure of the surgical wound.

Different designs exist for various surgical procedures, with the majority classified as either linear or circular [16].

When employing linear staplers, the surgeon utilizes the handles situated at one end to shut the "jaws" of the stapler at the opposite end over the tissue. Upon firing the stapler, a series of staples secures the tissue, and a blade cuts the tissue between the staples. This procedure effectively seals the open wound, preventing bleeding.

Linear staplers are employed to link tissue in minimally invasive surgeries or to extract an organ. Circular staplers are frequently utilized in surgeries related to the digestive tract, spanning from the throat to the colon.

Circular staplers discharge two staggered rows of staples from a circular cartridge. This configuration enables the stapler to join two segments of the intestine or another tube-like structure following the removal of a portion.

The staples result in the tissue gathering into rings or donuts between them. Subsequently, an integrated blade cuts off the overlapping tissue, finalizing the new connection. Surgeons monitor the closed wound for approximately 30 seconds to ensure proper compression of the tissue and verify the absence of any bleeding [11].

There are several types of surgical staples, each designed for specific purposes. Skin Staplers are used for closing skin incisions. They have a unique design with two prongs on each side of the staple, which helps distribute tension evenly across the skin. Linear staples are typically used for internal tissues, such as the stomach or intestines. They form a straight line of staples along the incision. Circular staplers create a circular pattern of staples and are commonly used

in gastrointestinal surgeries, particularly for creating anastomoses (connections between two parts of the gastrointestinal tract).

To achieve an ideal staple material, it is imperative to conduct degradation studies for confirming its stability. Two widely recognized standards for evaluating material degradation are ASTM F1635-04a and ISO 10993-13:2010. These standards assess degradation performance in physiological and oxidative wound environments, respectively [17].

In addition to the physical and chemical attributes of the staple material, it is equally essential to finely tune its biological properties to prevent significant biochemical processes that may lead to chemical leaching and the generation of toxic substances [18].

Biological properties should be tuned to prevent significant biochemical processes, chemical leaching, or the generation of toxic substances. Ideal staple materials should minimize such biological interactions.

Surgical staples are classified based on their fabrication materials and design. In terms of fabrication materials, they are broadly divided into metallic and polymeric staples. Metallic staples, including Stainless steel (SS), magnesium (Mg), zinc (Zn), titanium (Ti), and nickel-titanium (NiTiNol), offer strength and biocompatibility but face challenges such as corrosion, hydrogen gas production, and stress-induced corrosion [19] [20]. Polymeric staples, like PLA, PGA, and PLGA, are biodegradable and biocompatible but have lower mechanical strength than their metallic counterparts[21]. Notably, FDA-approved polymeric staples have shown promise in reducing operative time and improving patient compliance. The choice of staple design is also vital, with U-shaped and B-shaped designs being prevalent for their simplicity. The appropriate design selection depends on factors like tissue type, thickness, depth, and wound location. Ensuring proper design is essential to prevent undesirable deformation and achieve effective wound closure. Surgical staples made stainless steel and of titanium and titanium alloys are frequently used to repair the intestinal tract and the stomach[22]. Staples are used in gastrointestinal anastomosis to prevent surgical complications, shorten operating times, and ease patient suffering. However, the human body cannot absorb and hold onto these provided Ti essentials for an extended period. Furthermore, the Ti staples cause artefacts on

CT scans and other imaging tests, raising the possibility of a false positive. Conversely, a bioabsorbable staple composed of polymers that may break down in the environment of the human body serves as a substitute. Skin closure is currently offered with subcuticular absorbable staples made of polylactic and polyglycolic acid[23] .

Stainless steel (SS), titanium (Ti), and cobalt-chromium-molybdenum (CoCrMo) alloy are the most extensively used materials in biomedical engineering because of their biocompatibility and mechanical properties[24, 25] .

Austenitic stainless steel is commonly used in biomedical applications like surgical instruments and orthopedic implants due to its cost-effectiveness, ease of fabrication, biocompatibility, mechanical strength, and corrosion resistance[26-28].

Low carbon AISI 316L SS (meeting ASTM F138 and F139) with high molybdenum (2–3%) and chromium (17–20%) content, along with low carbon (less than 0.03%), is prone to increased local and intergranular corrosion[29].

Despite its common use in biomaterials and generally good biocompatibility, stainless steel (SS) lacks inherent bio functional properties like blood compatibility, osteoconductivity, and bioactivity due to the harsh conditions of the human body's biological environment[30] .

The adsorption of organic molecules, like proteins, on surfaces can trigger biofilm formation, potentially leading to corrosion or acting as a source of bacterial contamination[25] .

Furthermore, achieving additional bioactivity, such as drug release or selective cell capture, may be desirable. To attain these desired properties without compromising crucial bulk characteristics, stainless steel (SS) needs to be coupled with an active compound, such as a drug or antibody[31] . The bacterial infection on stainless steel is also noted as a significant drawback[32]

The residual tension left on the surface by stapling can affect the corrosion behaviour of the material in a physiological context. The number of research that consider this residual stress following staple insertion is very low[19]. It could be possible that material use for surgical

staple pins may corrode or degrade while the wound is still not properly healed. It is known that pins may act as a contact between the external environment and the tissues, muscles, and bones. So, infections can be one of the main complications[33] . Superficial infections are treated with local measures and oral antibiotics. If the infection progresses to the bones, causing pin loosening, more extensive measures like pin removal, replacement, and long-term intravenous antibiotic therapy are required, escalating both complexity and costs[34] .

Prior clinical studies have investigated various pin materials (ceramic, stainless steel, titanium) and coatings (hydroxyapatite, HA with FGF-2, silver, iodine). Despite extensive research on hydroxyapatite (HA) coating, the effectiveness of these materials in reducing infections remains unclear[34, 35] .

In most cases, surgical staples are designed to be left in place indefinitely and do not require removal. However, some staples used on the skin may need to be removed after a specific healing period, typically 7-14 days. A healthcare professional will remove them using a staple remover tool [36].

While surgical staples are widely used and generally safe, there can be complications, such as staple line leaks or infections. Surgeons meticulously assess staple selection considering the procedure, patient variables, and intended results.

In conclusion, surgical staples serve as invaluable instruments in contemporary surgical procedures, offering a prompt and efficient method for closing incisions and wounds. They are used across various medical specialties and have contributed to improved surgical outcomes and patient recovery times. The choice between staples and other closure methods, such as sutures or tissue adhesives, depends on the nature of the surgery and the surgeon's expertise [9].

2.2 Selection of materials

The materials are selected depending upon their properties which were desired for the composite material and ultimately the coating on Surgical staple pins.

The aim was to synthesize a composite material which when coated on our substrate will accelerate the wound healing process thereby helping in skin regeneration when applied on the wound plus it must improve corrosion resistance of the substrate. It must also bear antibacterial properties against specific bacteria. It must be strong enough against E. coli and S. aureus to prevent their growth or kill them.

2.2.1 Chitosan

We used a Chitosan as a matrix, while nHA and ZnO NPs were used as fillers. Chitosan was purchased through Sigma Aldrich while the nanoparticles of hydroxyapatite and zinc oxide were prepared through a specific synthesis route. Characterizations like SEM, XRD, FTIR were performed over the purchased and synthesized materials and then we proceeded towards the synthesis of our composite material and the coating.

Additionally, chitosan serves as an effective chelating agent owing to its capability to bind with cholesterol, fats, proteins, and metal ions. This chelating property makes it useful in various applications, such as water treatment and pharmaceutical formulations, where the removal or sequestration of these substances is essential [17, 18]

Nanofibers derived from chitin and chitosan, typically with diameters ranging from 50 to 500 nanometers, exhibit biocompatibility and biodegradability. This makes them well-suited for applications as hemostatic agents and wound healing materials [37].

Chitosan possesses notable antibacterial activity, as evidenced by studies. Furthermore, it demonstrates antifungal effects and exhibits mucoadhesive qualities [38]. Chitosan also offers analgesic properties and has been found to have hemostatic attribute [39].

Chitosan demonstrates biocompatibility when applied in various biomedical applications, including sutures and artificial skins, as supported by studies [38]. Importantly, it has received approval from the Food and Drug Administration (FDA) for use in wound dressings [40].

Chitosan, with its remarkable properties, is employed in a wide range of biomedical applications, including artificial skin, surgical sutures, controlled drug release systems, and even as an antibacterial agent [41].

Also, the Nano composite coatings having chitosan in them have been proved to improve the corrosion resistance of the substrate material [42, 43].

2.2.2 Bioactive Glasses (BG) / Nanohydroxyapatite (nHA)

The second material to be selected must have the properties to aid the soft tissue regeneration i.e, skin regeneration during the wound healing process. For that purpose, bioactive glasses play an important role. Bioactive glasses have shown the capability to expedite the process of skin regeneration by promoting angiogenesis and increasing collagen deposition during the proliferation stage, while also demonstrating beneficial impacts on the crucial phases of wound healing [44].

Bioactive glasses are capable of adhering to rigid tissues like bone, contributing to tissue regeneration through the creation of a calcium-phosphate-like layer on their surfaces. The development of this apatite layer facilitates a connection between the hard tissue and the glass, ultimately promoting bone healing [44].

Nonetheless, patients with compromised immune systems face a multitude of factors that contribute to slow healing, ultimately leading to the development of chronic wounds, particularly in diabetic individuals who are constantly at risk of inflammation and potentially life-threatening infections [45].

To facilitate the healing process, it becomes imperative to expedite blood clotting, prevent infections, and promote vascularization, as these three elements significantly influence the success of wound healing.

Ionically doped bioactive glasses (BGs) can accelerate these critical processes by incorporating various metallic oxides into the glass matrix to alter its chemical and physical properties. Subsequently, the release of ions as a result of the dissolution of the glass in biological

environments can bestow hemostatic qualities (e.g., Ca^{2+}) and antimicrobial attributes (e.g., Ag^+ and Cu^{2+}) [46-48].

The potential of bioactive glasses (BGs) to stimulate angiogenesis presents an attractive alternative to the expensive growth factors traditionally utilized to stimulate the development of new blood vessels in damaged tissues.

Recently, BGs have found application in wound treatment and have exhibited significant potential in the realm of wound healing. Some specific BG compositions can be employed to accelerate the healing process by assisting in the various stages of wound recovery [44].

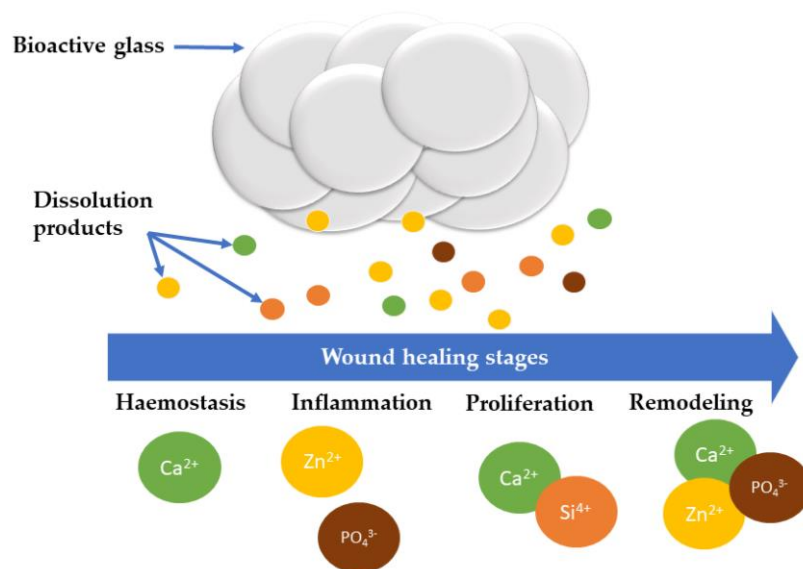


Figure 4: Wound Healing Stages on Bioactive Glass

Bioactive glass (BG) appears to promote wound healing, in part, by influencing and regulating the inflammatory responses during the wound healing process. It also plays a role in enhancing the paracrine interactions between macrophages and the cells involved in the repair process [49].

In short, bioactive glasses have a diverse range of potential applications in wound healing, from enhancing fibroblast activity and angiogenesis to modulating inflammatory responses and promoting hemostasis. These findings hold promise for the development of innovative biomaterials to improve wound care and healing in various clinical settings [44].

Rather than using bioactive glasses or synthesizing them, we decided to use something that work same as they do.

Biomaterials play a crucial role in the field of medicine by providing non-living materials that can be used to restore or replace dysfunctional tissues and organs. Over the last half-century, there has been significant progress in the science and engineering of biomaterials, driven by substantial investments in the development of innovative products [50].

Biomaterials can be categorized into two main types: natural and synthetic materials. As previously mentioned, the survival of stem cells necessitates a specific environment. Therefore, biomaterials provide a promising approach to replicate the *in vivo* microenvironment, enabling the regulation of stem cell destiny through interactions with the cell-matrix [51].

We decided to use nano-hydroxyapatite instead of the bioactive glasses as it disassociates as Calcium and phosphate ions just like bioactive glasses breaks as the pH increase.

In the pursuit of emulating the 3D extracellular matrix (ECM) to influence stem cell behavior, various natural biomaterials have been employed to facilitate stem cell proliferation and differentiation. These materials encompass a range of substances such as collagen, gelatin, hyaluronic acid hydrogels, fibrin, glycosaminoglycans (GAGs), alginate, matrigel, silk, and hydroxyapatite (HA), among others [50].

nHA serves as a source of localized calcium delivery, on the growth, proliferation, differentiation, and extracellular matrix production of human dermal fibroblasts, keratinocytes, and human mesenchymal stem cells (hMSCs) [52].

the provision of calcium ions by nanoHA had a significant positive effect on cellular growth and proliferation rates. Additionally, it exhibited a preventive action against the adhesion of

pathogenic bacterial strains commonly found in the human skin flora. Furthermore, hMSCs exhibited the capability to differentiate into both osteogenic and adipogenic lineages [53].

Moreover, hydroxyapatite has considerably good corrosion resistance properties antibacterial, wound healing properties. When incorporated with other material i.e; forming a composite with other materials considerably enhanced properties are observed [53, 54].

Therefore, the selected material nHA was synthesized through a specific synthesis route.

2.2.3 Zinc Oxide Nanoparticles (ZnO)

The third material selected was the zinc oxide nanoparticles because of their good wound healing antibacterial properties. When they are coated over a substrate, they enhance the corrosion resistant properties [55]. Zinc oxide nanoparticles exhibit several distinct properties, including luminescence, the release of Zn^{2+} ions in aqueous environments, particularly in acidic conditions, generation of reactive oxygen species (ROS), especially upon exposure to UV light, versatile surface chemistry, and a straightforward and cost-effective synthetic process that enables precise control over particle size and shape.

These characteristics render zinc oxide nanoparticles a highly versatile material, whether used independently or in conjunction with other elements. Consequently, ZnO nanodevices find applications across a wide spectrum of scientific domains, with a particular emphasis on biomedicine. The latest developments stemming from their utilization in the treatment of cancer and diabetes, their effectiveness against bacteria, fungi, and inflammation, as well as their potential in wound healing [56].

A noteworthy characteristic of ZnO nanomaterials is their low toxicity and biodegradability. Zn^{2+} is an essential trace element for adults, participating in a range of metabolic processes. The recommended daily intake of Zn^{2+} is 11.0 mg for adult men and 9.0 mg for adult women in the United States. Furthermore, ZnO surfaces are chemically rich in -OH groups, which can be easily modified or functionalized with various surface-binding molecules [57, 58].

Moreover, its composite with other materials further resulted in enhanced properties, like antibacterial, corrosion resistance etc. [54].

Therefore, the selected materials were Chitosan, nanohydroxyapatite and zinc oxide nanoparticles depending upon their required properties.

Chapter 3:

Materials and Methods

3.1 Synthesis route:

There are many methods/approaches that could be used to synthesize the nanoparticles and nanocomposite coating. There are two approaches that have been used to synthesize nanoparticles and these are, top-down approach and bottom-up approach. Top-down methods include lithography, milling, and repeated quenching. An inherent limitation of this method is its lack of effective control over both the structure and particle size. The bottom-up approach is widely employed in nanoparticle synthesis, wherein the material is constructed incrementally, proceeding from atoms, molecules, to clusters. In this approach, chemical reactions are used to synthesize the materials in a bottom-up approach. Various metal nanoparticles are synthesized through the reduction of metal salts by. To synthesize Zinc oxide nanoparticles, hydroxyapatite nanoparticles and Chitosan - hydroxyapatite - zinc oxide composite wet- chemical synthesis (a bottom up approach) was used.

3.1.1 Wet- chemical synthesis

Targeted material is prepared by adding precursor into a specific solvent and the reaction takes place within the solution. Surfactants or capping agents are used which serve to regulate the size, shape, and structure of the targeted product. The most extensively used wet chemical processes for the nanomaterials' synthesis are Template synthesis, hydrothermal synthesis, solvothermal synthesis, self-assembly of nanocrystals, soft colloidal synthesis etc [59].

Advantages:

- Wet chemical techniques are better at controlling the shape of nanomaterials.

Disadvantages:

- A single layer of 2D nanosheets is difficult to obtain/achieve.

The wet chemical method is used for the synthesis of both metal oxide nanoparticles and hydroxyapatite nanoparticles because of the controlled size, form, and morphology of the desired product.

3.2 Methods for coatings

There are a variety of coating methods containing different coating materials, for different coating applications. Available coating materials encompass rigid and durable metallic alloys, bio-glasses, ceramics, polymers, and other engineered plastics. These materials provide freedom to choose accordingly. There are various coating methods that have been introduced and investigated, and these are [60, 61]:

- Chemical/Physical Vapour Deposition
- Micro-arc oxidation
- Sol-gel
- Thermal spraying
- Spin coating
- Electro-deposition coating

3.2.1 Electrodeposition Coating

It is the deposition of metallic ions on the substrate, which involves an ion transfer in a unit cell due to potential difference between cathode and anode poles. Over time, a layer of coating is developed on the submerged substrate by receiving ions from the opposite electrode. [62]. It has two types:

- Electrolytic deposition (ELD)
- Electrophoretic deposition. (EPD)

3.2.1.1 Electrolytic deposition

It is an electrochemical procedure employed to create a dense metallic coating with a uniformly distributed thickness on a substrate, and substrate should be conductive. The substrate and the materials for deposition are designated as the cathode and anode, respectively, and are positioned within an electrochemical unit cell. Potential difference is applied between both poles and the metallic ions thus move towards the substrate through working electrolyte.

The concentration of metallic ions in the electrolyte remains consistent.

Advantages:

- Decorative and high corrosion resistance
- High temperature applications, wear applications. (46, 47 ref. from paper)

Disadvantages:

- Works for conductive substances/substrates.

3.2.1.2 Electrophoretic deposition

It's a multiphase technique in which using an electric field like ELD, thin films are formed on the substrate by clotting of colloidal particles [63-65].

- The external electric field drives suspended particles of electrolyte to either the cathode or anode through electrophoresis.
- These particles start to accumulate in one of the electrodes and thus form a coagulated particle.
- The larger particles are deposited on one of the electrodes, which would be our to-be-coated substrate.

Advantages:

- Up till now, EPD has various applications that may include coating, selective deposition, biomedical application and many more. Borides, carbides, oxides, phosphates, metals etc. are commonly used in EPD.

Disadvantages:

- Works for conductive substances/substrates.

3.3 Aims and Objectives

The aim of this study is the surface modification of surgical stapler pins (SSPs) made of Stainless steel 316L for biomedical applications. It includes:

- Synthesis of zinc oxide (ZnO) nanoparticles via wet-chemical process.
- Synthesis of hydroxyapatite nanoparticles (nHA) via wet-chemical process.
- Synthesis of nanocomposite coating using ZnO, nHA, chitosan.
- Deposition of coating via electrophoretic deposition method.
- Corrosion resistance testing of the prepared coated material.
- Antibacterial testing of the prepared coated material.
- Furthermore, this product will help to accelerate the wound healing process and can be used in emergency medical situations.

3.4 Synthesis of ZnO Nanoparticles:

Zinc oxide nanoparticles were synthesized by wet-chemical method by using Zinc Nitrate ($Z(NO_3)_2 \cdot 6H_2O$) and Sodium Hydroxide (NaOH) as precursors. In this experiment, 0.1M solution of zinc nitrate was magnetically stirred to completely dissolve zinc nitrate in DI water for almost 1hr. 1M aqueous solution of NaOH was prepared in the same way and stirred magnetically for 1hr. 1-2mL acetic acid is used as a capping agent. After the complete dissolution of zinc nitrate, 1M NaOH was added drop by drop under constant stirring till the solution turns milky. pH was checked time to time and should be between 7- 12. As the solution

turns milky, stop further addition of NaOH. The reaction was allowed to proceed for 2 hrs at 90 °C. After the completion of reaction, the beaker was sealed, and the solution was allowed to settle down overnight at room temperature.

The supernatant solution was separated carefully, and the remaining solution was centrifuged at 4000 rpm for 20 mins. The precipitates were removed and further cleaned by washing with Deionized water and ethanol to remove by-products if left any with the NPs. The Nano particles were then dried at 60 °C. During this process, Zn (OH)₂ is converted into ZnO. After drying the particles were annealed for 4hrs at 350 °C. The prepared ZnO nanoparticles were then characterized through FTIR, XRD and SEM [66].

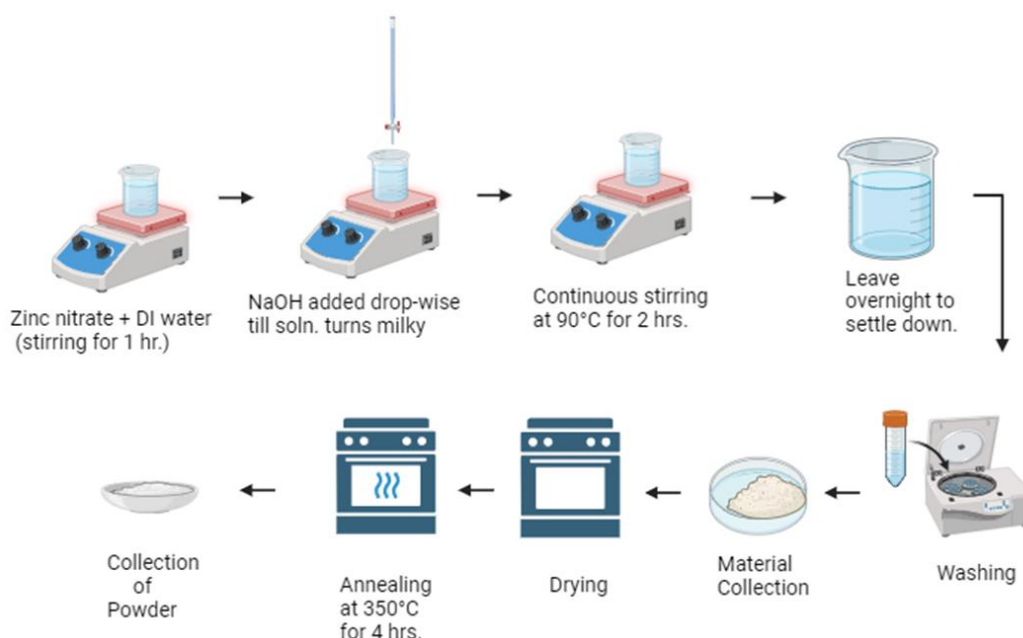


Figure 5: Synthesis of Zinc Oxide Nanoparticles

3.5 Synthesis of Hydroxyapatite Nanoparticles (nHA)

Wet-chemical method was used to prepare the Hydroxyapatite nanoparticles. nHA was prepared by using Diammonium hydrogen phosphate (NH₄)₂HPO₄ as a source of phosphorous, Calcium nitrate tetrahydrate (Ca (NO₃)₂ .4H₂O) as a source of calcium and ammonia solution as an agent to control pH. 55 mL of distilled water was used to dissolve 3.8 grams of

diammonium hydrogen phosphate with continuous stirring at 80 °C until the whole salt was dissolved. Ammonia solution was added to adjust the pH up to 12. 13g of calcium nitrate tetrahydrate was dissolved separately in 80mL distilled water at 80 °C under continuous stirring until the salt was dissolved. $(\text{Ca}(\text{NO}_3)_2 \cdot 4\text{H}_2\text{O})$ solution was added drop by drop in $(\text{NH}_4)_2\text{HPO}_4$ solution under continuous stirring and the resultant solution was subjected to stirring for 2 hrs at 80 °C. Rate of reaction must be controlled for the desired crystal structure.

After the completion of reaction, the beaker was sealed, and the solution was left to settle at room temperature for particles to precipitate. After that, washing with distilled water and ethanol was done. The powder was then collected and dried at 80 °C for 24 hrs for the removal of any by-products. It was then calcinated at 850 °C for 3hrs. The prepared hydroxyapatite nanoparticles were then characterized through FTIR, XRD and SEM.

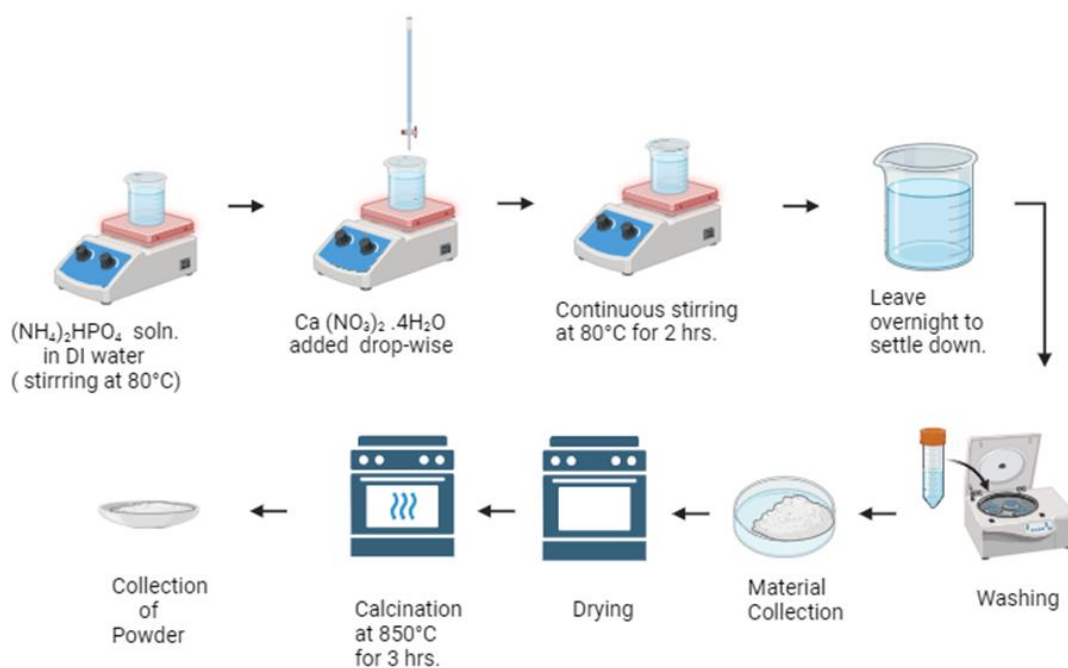


Figure 6: Synthesis of Nanohydroxyapatite

3.6 Selected Coating Method

Electrophoretic deposition method was selected for the synthesis and deposition of our coating because of the flexibility in the selection of materials and its applications in biomedical. For this purpose, a suspension was prepared by adding our synthesized nanoparticles along with other materials and specific solvents. Following is the method for the suspension preparation.

3.6.1 Suspension preparation

Chitosan, Zinc oxide NPs, Hydroxyapatite NPs, distilled water, and ethanol were used to prepare the suspension, while acetic acid is used as an agent to control the pH which should be less than 6. A suspension of 10mL was prepared by adding in 1.6mL distilled water in 8.2mL ethanol with further addition of 0.2mL acetic acid and the whole solution was stirred continuously at 30°C. After that 0.025g of Chitosan was added to the prepared solution and stirred magnetically for 30 mins and ultrasonically dispersed for 10 mins. In the next step, 0.0025g of HA nanoparticles were added to the solution and magnetically stirred for 6 hrs at 30°C and ultrasonically dispersed for 10 mins.

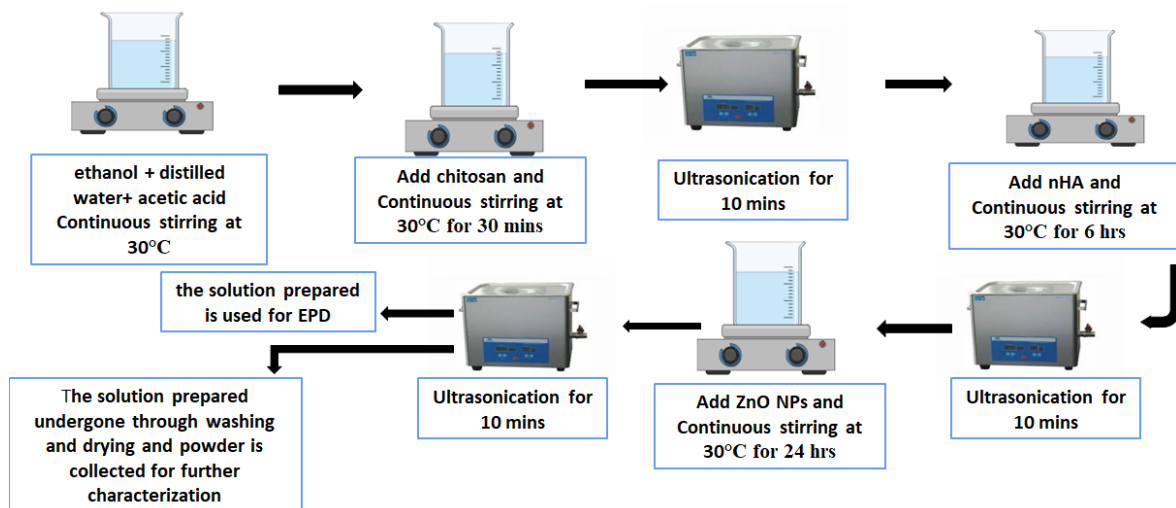


Figure 7: Suspension Preparation

Finally, to prepare the three-component suspension 0.01g of ZnO nanoparticles were added to the two- component suspension (0.025g Chitosan, 0.0025g HA NPs) and magnetically stirred

for 24hrs followed by the ultrasonically dispersion of 10mins. The powder was extracted by centrifugation of the suspension, washing the obtained powder with distilled water (2 times, 4000 rpm) and then drying them at 80 °C. The obtained powder was then characterized through FTIR, XRD, SEM.

3.7 Electrophoretic deposition

The Surgical staple pins (SSPs) of 316L stainless steel were used as a substrate as well as the counter electrode in EPD cell. SSPs were first attached to silver/copper wire and then to the terminals of the DC power supply through crocodile clips. The applied voltage between the electrodes was 15V and the deposition time was 3mins. Four suspensions were prepared: three -one component suspensions having chitosan, HA NPs and ZnO NPs alone, and one - three component suspension having chitosan, HA NPs and ZnO NPs altogether. The samples were dried at room temperature and are characterized by FTIR, XRD, SEM.

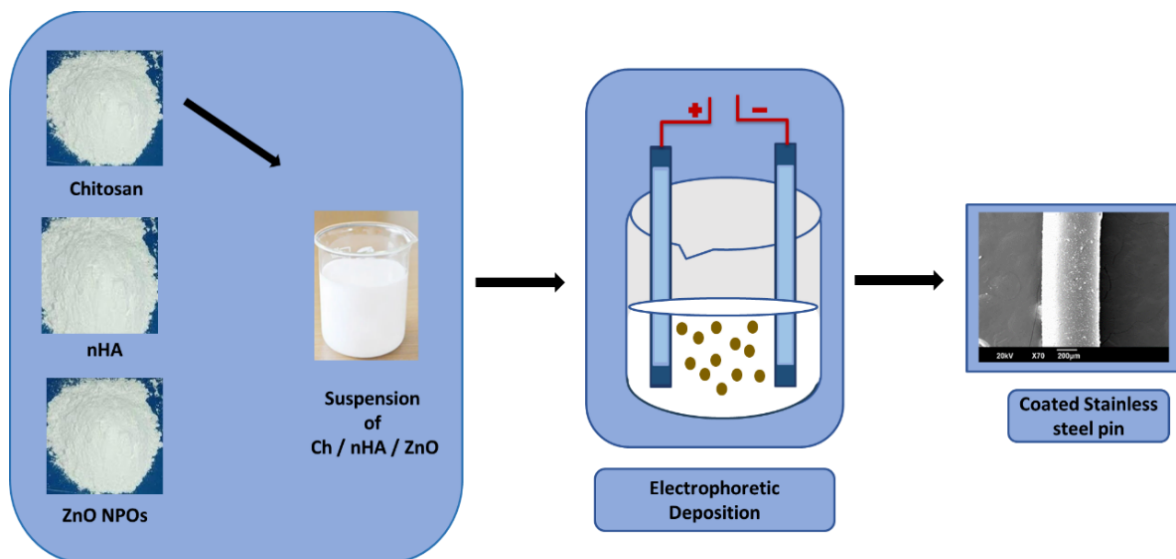


Figure 7: Electrophoretic Deposition

Chapter 4:

Characterization Techniques

4.1 Scanning Electron Microscope (SEM)

A fine beam of electrons is focused over the surface of a specimen in this technique. As a result, photons or electrons are ejected from the material's surface. The electrons that have been knocked off are then focused on the detector. The detector's output modulates the brightness of the cathode ray tube (CRT). A subsequent point on CRT is plotted for each point where the beams interact, and the material's image is produced [67].

The interaction between electrons and surfaces leads to the emission of secondary electrons (SE), backscattered electrons (BSE), and X-ray [68]. Secondary electrons are a common form of detection for SEMs. These electrons are discharged from the sample's surface. Thus, a clear and pronounced image of the sample is obtained. It can disclose sample information as little as 1 nm. Also, incident electrons undergo elastic scattering and liberate backwards scattered electrons. They originate from deeper sites than secondary electrons. Therefore, their resolution is relatively low. When an inner shell electron is ejected from its shell, distinctive x-rays are emitted [69].

We employ SEM because it allows us to determine important characteristics about our samples, including their morphology, chemistry, crystallography, and plane orientation quickly and easily. The SEM may be adjusted to any magnification between 10 and 500,000 times.

FESEM analysis and morphological examination of the materials were conducted on a (JEOL-JSM- 6490LA) (MIRA3 TESCAN). The elemental make-up was analysed with the use of an EDS detector coupled to a FESEM.

4.2 X-RAY Diffraction (XRD)

It is used to determine the material's crystal structure. It is a non-destructive technique that provides fingerprints of crystalline materials' Bragg reflections. It comprises of three major components. A detector, sample container/holder, and cathode tube. Heating a filament element accelerates electrons towards a target, where they clash with target material to create X-rays. Crystal consists of several layers and surfaces. Therefore, x-rays with wavelengths comparable to these planes are reflected so that the angle of incidence equals the angle of reflection. The phenomenon of "diffraction" is described by Bragg's Law:

$$2d\sin\theta = n\lambda$$

When Bragg's law is satisfied, it means there is constructive interference, and "Bragg's reflections" will be picked up by the detector. These reflections positions tell us about inter-layer spacing-ray diffraction tells us about the phase, crystallinity, and sample purity. By this technique, one can also determine lattice mismatch, dislocations, and unit cell dimensions.

X- ray diffractions were performed by STOE diffractometer at SCME-NUST. The scan angle was taken between 5° to 90° [70].

4.3 Fourier Transform Infrared Spectroscopy (FTIR)

It is a physio chemical spectroscopic technique which helps in determining the functional groups of organic and non-organic compounds by determining their vibrations. When the material is exposed to IR radiation, the molecules in it get excited and show different vibrations in different frequency ranges. In case of composites, FTIR helps in determining the presence of fillers as well as chemical bonding of materials [71].

In electromagnetic spectrum, infrared region lies in the range of (14000-10) cm^{-1} and can be further divided as:

- Near IR (400-10) cm^{-1}

- Mid IR (4000-400) cm^{-1}
- Far IR (14000-4000) cm^{-1}

Mid IR region is also called finger-print region. The IR active molecules show their characteristic primary vibrations in this region which ultimately helps in determining/identifying the functional groups.

In this technique, the analyte is exposed to the range of wavelengths and the molecular bonds show absorbance at specific wavelengths undergoing excitation which further leads to vibrations. These vibrations could be stretching and bending. Bending vibrations are also called contractions. The IR spectrum is plotted between wave numbers on X-axis while absorbance or transmittance on Y-axis. It follows Beer-Lambert law,

$$A = \epsilon.C.l$$

Where, A= absorbance, ϵ = molar absorptivity, C= concentration, l = path length.

4.4 Electrochemical Workstation

Biologic VSP is the research-grade potentiostat present at SCME. Equipment consists of workstation, electrochemical cell, computer hardware, and software system. It is used for many applications including:

- Battery testing
- Fuel cell and biofuel cell
- Liquid conductivity
- Electrochemical deposition of thin film
- Material impedance spectroscopy
- Corrosion testing

- Photovoltaics and sensors
- Capacitor and supercapacitor testing
- Electrochemical Impedance Spectroscopy (EIS)

Corrosion testing was performed in our case along with electrochemical impedance spectroscopy EIS.

4.4.1 Corrosion testing

Accelerated electrochemical corrosion was performed on coating substrate system to evaluate it in different stimulate environments. Different solutions can be used to stimulate certain type of environments depending upon the areas of application such as, 3.5% NaCl solution is used as an electrolyte to provide the marine environment and 0.2 molar aqueous solution of Na₂SO₄ can be used to provide industrial environment. However, our area of application is the human body so in our case Hank's solution was used to stimulate the required environment. The pH of this solution should be between 6.8-7.2. This solution was prepared in lab by a specific synthesis route.

4.4.2 Hanks's Solution

To prepare Hank's Balanced Salt Solution (HBSS), begin by setting up an 800 mL container filled with distilled water. First, add 8 g of Sodium chloride to the solution, followed by 0.4 g of Potassium Chloride, 0.14 g of Calcium Chloride, 0.1 g of Magnesium Sulfate Heptahydrate, and 0.1 g of Magnesium Chloride Hexahydrate. To this mixture, incorporate 0.06 g of Sodium Phosphate Dibasic Dihydrate and 0.06 g of Potassium Phosphate Monobasic. Ensure the solution's vitality by adding 1 g of D-Glucose (Dextrose) and 0.35 g of Sodium bicarbonate. The final step is to adjust the volume to 1 liter (1 L) by adding additional distilled water. The resultant after continuous stirring is Hank's solution.

Hank's Balanced Salt Solution (HBSS) is a versatile buffer solution widely utilized in various scientific and medical applications, with corrosion testing being just one of its many uses. From

a medical perspective, HBSS is essential due to its ability to mimic the physiological environment within the human body. This balanced salt solution contains essential salts, minerals, and glucose, making it an ideal medium for maintaining cells and tissues in a healthy state during experiments and medical procedures.

In corrosion testing, HBSS serves as a valuable tool to evaluate the compatibility and longevity of medical implants and devices within the human body. By subjecting these materials to the simulated physiological conditions provided by HBSS, researchers can assess their resistance to corrosion and degradation, ensuring the safety and effectiveness of medical devices like orthopedic implants, stents, and prosthetics. The use of HBSS in corrosion testing is pivotal in upholding the high standards of safety and performance in the field of medical technology, ultimately benefiting patients and healthcare practitioners alike.

4.5 Antimicrobial testing

Antimicrobial susceptibility testing has applications in drug discovery, epidemiology, and therapeutic outcome prediction. A lot of methods can be used to perform the in vitro antimicrobial activity of material. Common methods for antimicrobial testing include the disk diffusion method and broth or agar dilution methods. Diffusion methods encompass agar disk diffusion, antimicrobial gradient methods (e.g., Etest), agar well diffusion, agar plug diffusion, cross streak method, and poisoned food methods. Dilution methods involve broth dilution and agar dilution. Additional techniques, like poisoned food methods, can be employed for antifungal testing [72].

4.5.1 Diffusion method

Diffusion is the movement of molecules from the area of higher concentration to the area of lower concentration. Diffusion methods in antimicrobial activity basically disk diffusion methods. The disc diffusion method (DDM) falls under agar diffusion methods (ADM), where the tested substance diffuses from a reservoir, typically a filter paper disc, across agar medium inoculated with the test microorganism. After incubation, a zone of inhibition forms around the

disc if the tested material is microbiologically active. The diameter of this zone indicates the antimicrobial effectiveness of the substance. [72-74].

4.5.2 Dilution method

The dilution test determines the minimum concentration (in mg/ml) of an antimicrobial agent needed to inhibit or kill bacteria. This involves applying varying dilutions of the antimicrobial agent directly to an agar pour, a broth tube, or a micro-broth panel. The lowest concentration that prevents observable growth of the organism is referred to as the Minimum Inhibitory Concentration (MIC)[75].

Dilution and diffusion methods are further subcategorized depending upon the protocols.

4.5.3 Colony Forming Unit (CFU)

CFU can be used to find or check the antibacterial activity of the coatings. CFU stands for "Colony Forming Unit." It is a term commonly used in microbiology to quantify the number of viable microorganisms, such as bacteria or yeast, in a given sample [76].

A single CFU represents one microorganism or a group of microorganisms that are capable of forming a visible colony when grown under specific conditions, such as on a solid agar medium.

Counting CFUs is a fundamental method for determining the concentration or density of viable microorganisms in a sample and is widely used in research, quality control, and clinical microbiology [77, 78].

The Colony Forming Unit (CFU) method is a widely used technique to assess the antibacterial or antimicrobial activity of coatings. Here's how it typically works:

First, the coatings that are to be tested for their antibacterial properties are applied to substrates or surfaces. These coatings may contain antibacterial agents, such as nanoparticles, chemicals, or other substances.

Known quantities of bacteria (usually pathogenic or target bacteria) are inoculated onto the coated surface. The bacteria are evenly spread, and the sample is left to incubate.

The coated samples with the bacteria are incubated under controlled conditions. This allows the bacteria to grow and form colonies on the coated surface.

After the incubation period, the samples are assessed to determine the quantity of bacterial colonies present on the coated surface. This is typically done by visual inspection, or in some cases, with the help of automated image analysis.

The number of bacterial colonies (CFUs) is counted and recorded. CFU refers to the colony-forming units, and it represents viable bacteria capable of reproducing.

The CFU count on the coated surface is compared to a control or untreated surface. This comparison allows for an assessment of the antibacterial efficacy of the coating.

The CFU method provides a quantitative measure of the coating's ability to inhibit bacterial growth and is a standard approach for evaluating the antibacterial effectiveness of various materials, including coatings used in medical devices, food packaging, and other applications where bacterial contamination is a concern [78].

Chapter 5:

Results and Discussion

5.1 X-Ray Diffraction

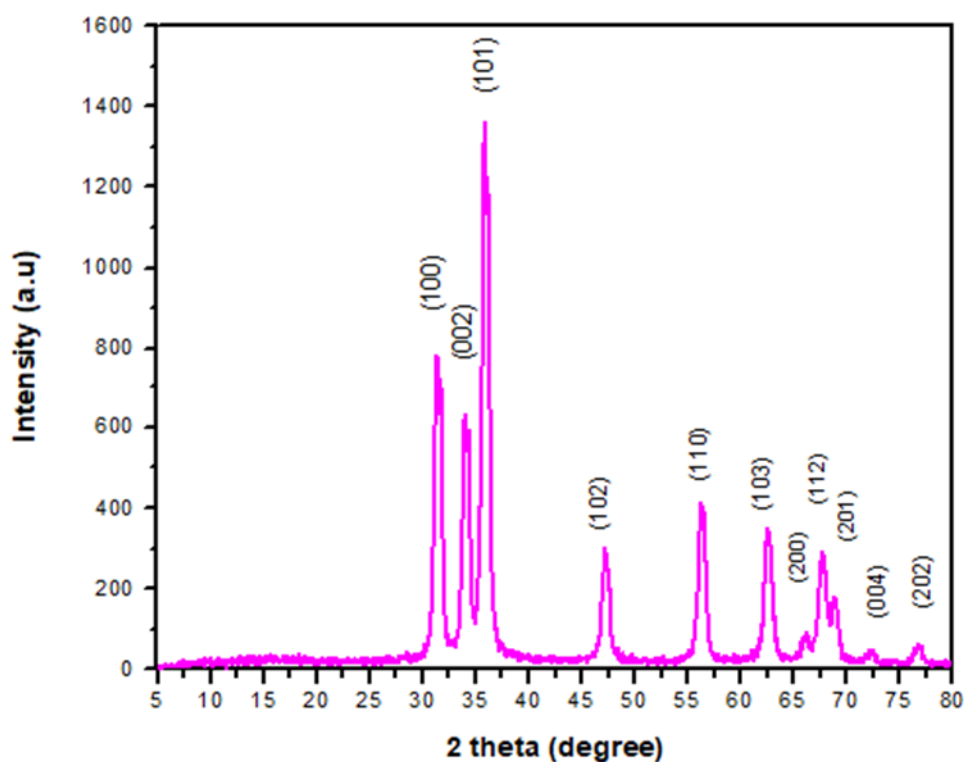


Figure 4: XRD of ZnO NPs

Figure 8 shows the XRD of ZnO nanoparticles. The ZnO exhibited distinct diffraction peaks, confirming its crystallinity. The XRD pattern of ZnO nano particles contains 11 prominent diffraction peaks. All these peaks correspond to Bragg reflections (100), (002), (101), (102), (110), (103), (200), (112), (201), (004), and (202). The observed reflections are in good agreement with the reference code 36-1451 [79].

The Debye-Scherrer equation, also known as the Scherrer equation, was used to estimate the average crystallite size of a material based on the broadening of X-ray diffraction peaks.

The crystal structure was wurtzite hexagonal. The crystallite size was 40.3 nm.

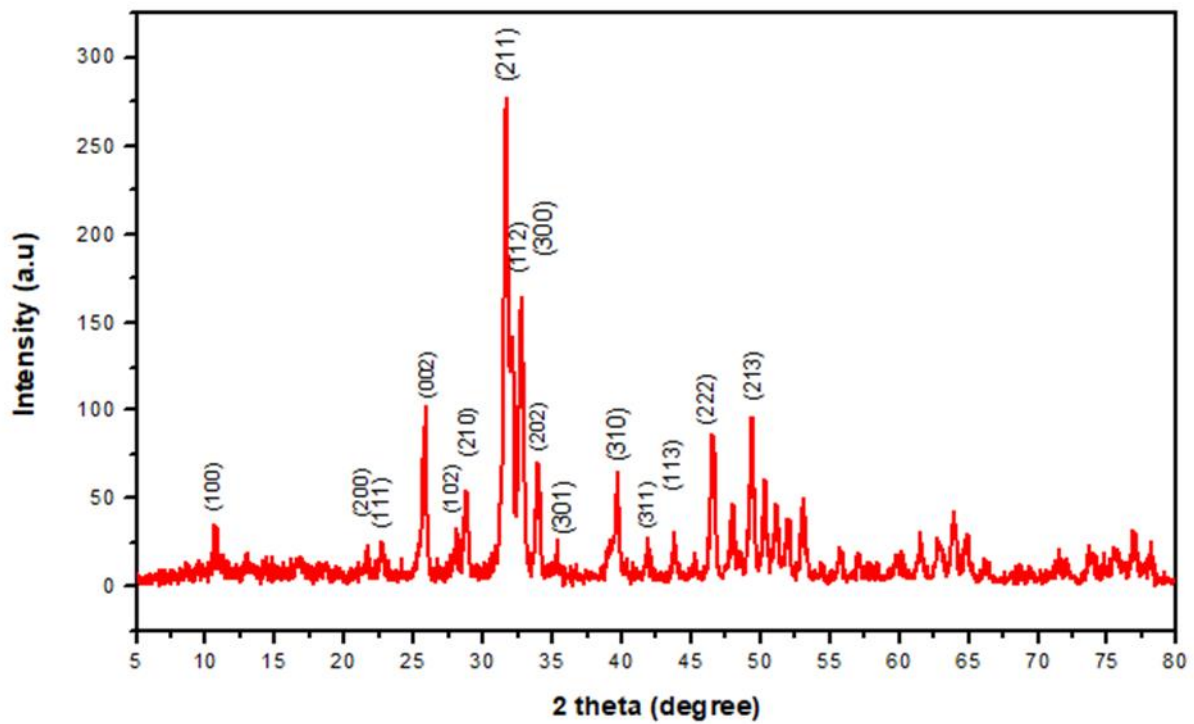


Figure 5: XRD of nHA

The graph demonstrated that nHA has 16 distinct peaks. The diffraction pattern matches reference code 0240033 quite well. The characteristic peaks are (002), (211), (112) and (113). The crystallite size calculated through Debye-Scherrer equation turned out to be 27.23 nm [80].

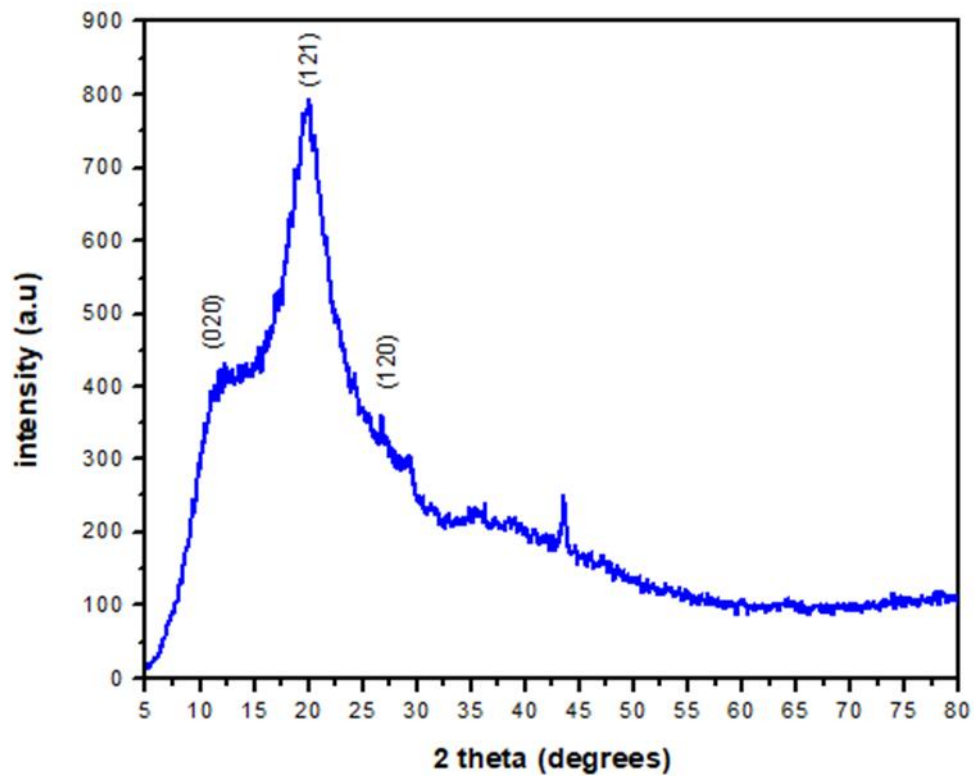


Figure 6: XRD of Chitosan

The powder XRD graph of chitosan shows 3 prominent peaks which are indexed as (020), (121) and (120). The XRD pattern is in accordance with JCPDS card number 39-1894. The crystallite size was 19.5 nm [81].

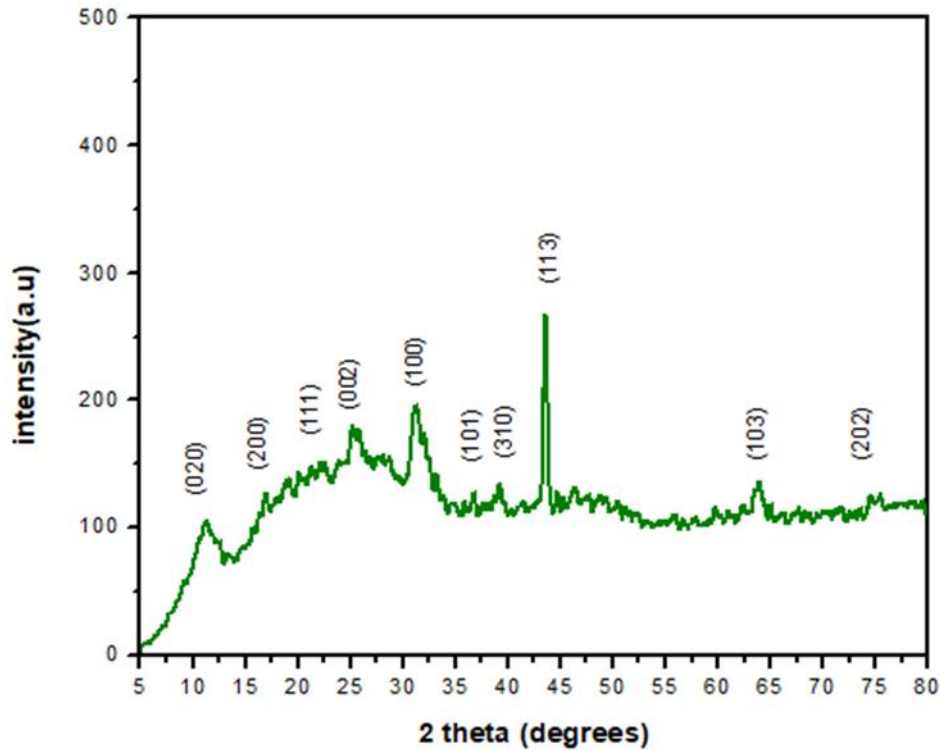


Figure 7: XRD of Ch/ nHA/ ZnO

The figure depicts the XRD pattern of composite. Chitosan is present in the composite and is indicated by the peaks at 11.5 and 19.1o, which are indexed as (020) and (121) respectively. The diffraction peaks 25.2, 39.4, and 43.6o correspond to nHA with diffraction plans (002), (310), and (113). The peaks observed at 31.5, 36.5, 64.3 and 68.1o attributed to ZnO and indexed as (100), (101), (103) and (202) respectively. The characteristics peaks of chitosan, nHA, and ZnO are present and confirmed the successful formation of composite.

5.2 Fourier Transform Infrared Analysis

The FT-IR spectra of chitosan was observed within the range of 4000 cm^{-1} to 500 cm^{-1} . The infrared spectrum for chitosan is shown in the fig. The peak around 3448 cm^{-1} is attributed to the stretching vibrations of -OH bond overlap with N-H stretching vibration in chitosan [82,

83]. The peaks observed around 2924.13 cm^{-1} showed stretching vibrations for that for C–H bond.

The absorption peaks observed at various wavenumbers, such as 1656.88 cm^{-1} , 1571.05 cm^{-1} , 1422.53 cm^{-1} , and 1378.16 cm^{-1} , are indicative of specific molecular vibrations. Specifically, these peaks are associated with the C=O stretching of the amide I band, bending vibrations of the N–H (in N-acetylated residues, corresponding to the amide II band), C–H bending, and OH bending, respectively.

Additionally, the peak at 1157.31 cm^{-1} is attributed to the anti-symmetric stretching of the (C–O–C) bridge, while the peaks at 1075.33 cm^{-1} and 1025.18 cm^{-1} are linked to the skeletal vibration involving C–O stretching [84].

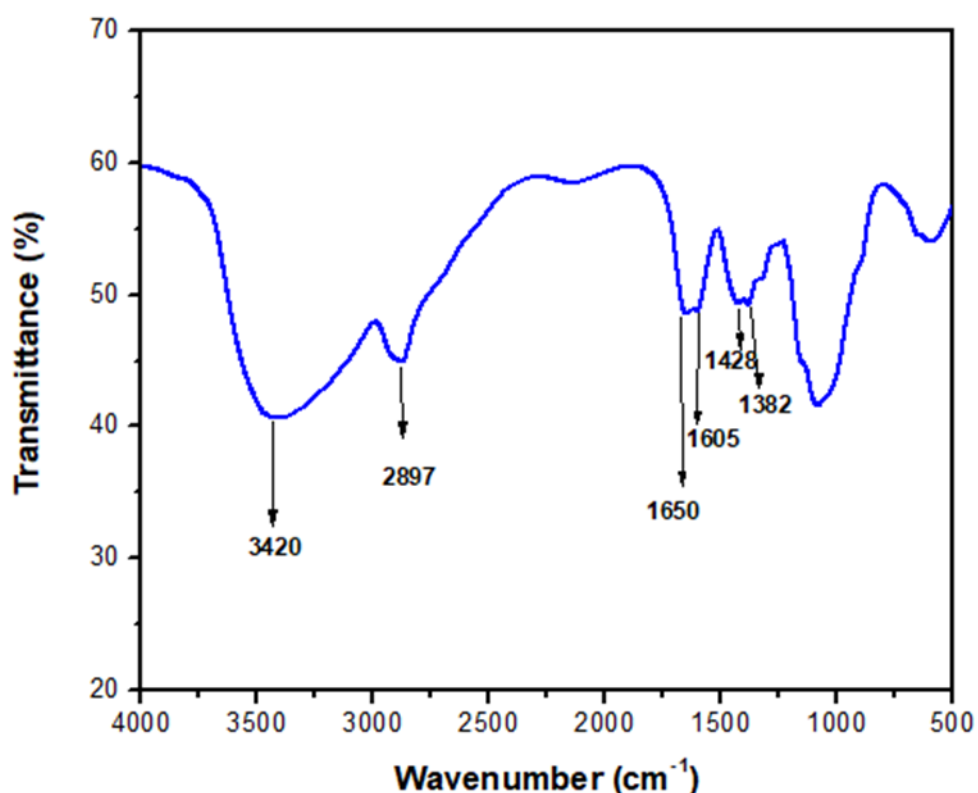


Figure 8: FTIR of Chitosan

The Fig shows the FTIR analysis of ZnO NPs.

FT-IR transmission spectra of ZnO NPs in the 500–4000 cm^{-1} range were measured. (Main) The peak around 3437.8 cm^{-1} represents the stretching vibration of O-H bond. This may be due to the oscillations of water molecules [85-88].

The peak observed at 2925.8 cm^{-1} was related to $-\text{CH}_2$ vibration [85, 89]. The transmission peaks observed around 1595 cm^{-1} were due to C=O symmetric stretching [89]. The transmission peaks observed at 1383.5 cm^{-1} and 1355.5 cm^{-1} were bending vibrations, and these are the vibrational modes of CO_2 [90]. The peak at 1005.3 cm^{-1} is related to H-O-H bending vibration. It is mainly due to the presence of water of crystallization [89]. The peak observed around 863.3 cm^{-1} was also due to the deformation vibration of water molecules [88, 91]. The transmission band observed at 575.9 cm^{-1} was due to Zn-O stretching modes.

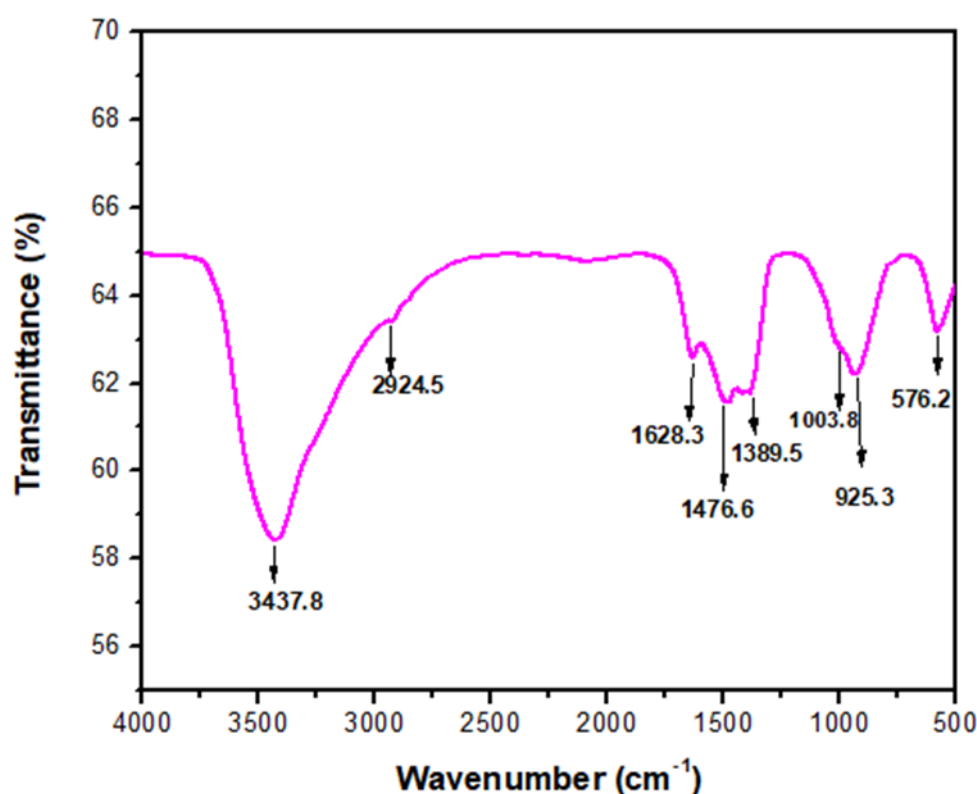


Figure 9: FTIR of ZnO

The figure shows the FTIR spectra of the prepared sample nHA. The peak observed around 3568 cm^{-1} is the ion stretching vibration and confirms the presence of a hydroxyl group, OH^- [92, 93]. The stretching vibrations of carbonyl groups and phosphate groups were also observed [94]. The peak at 1461 cm^{-1} shows the asymmetric stretching of CO_3^{2-} . The peak observed around 1041 cm^{-1} is the asymmetric stretching of PO_4^{3-} . The peak at 869 cm^{-1} is the bending mode of CO_3^{2-} , which is out of plane bending. The peak at 570 cm^{-1} shows the asymmetric bending vibration of PO_4^{3-} [95, 96].

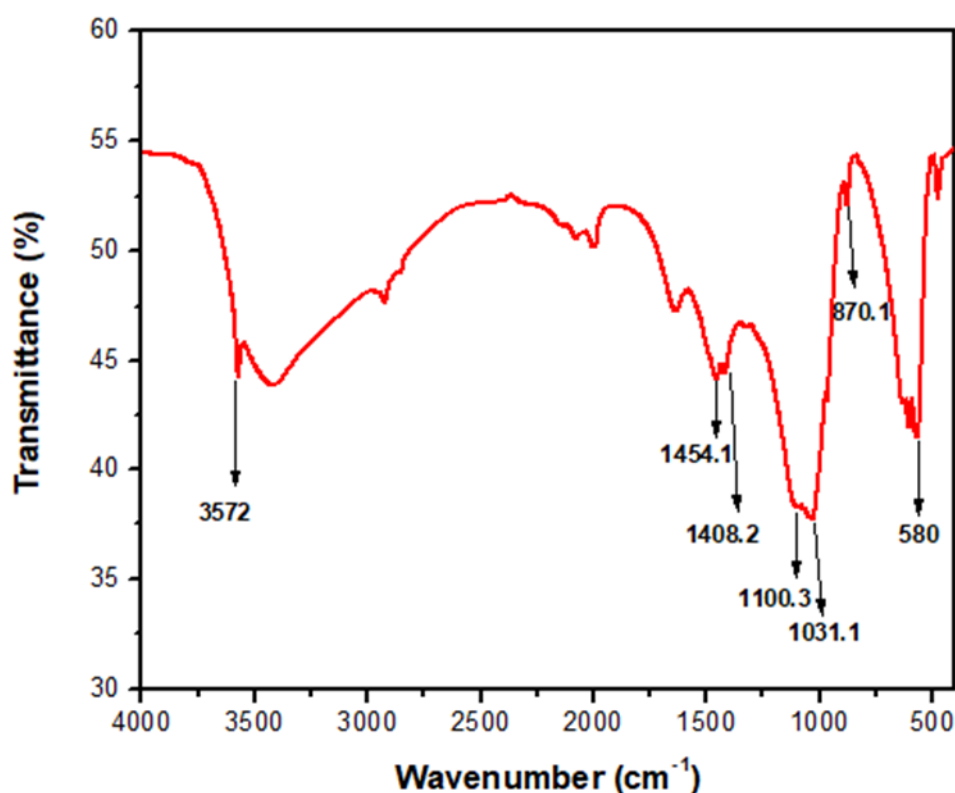


Figure 10: FTIR of nHA

The FTIR spectra of the composite material in fig 15 showed the presence of the characteristic bands that were present in the individual IR spectra of the individual materials Chitosan, nHA, ZnO with minor shifts of the peaks is observed. The peak broadening around 3400 cm^{-1} observed which showed the interaction of NH and OH groups of Chitosan, nHA, and ZnO. The peaks observed around 2978.6 cm^{-1} and 2829.8 cm^{-1} showed the stretching

vibrations for that for C–H bond. Similarly, the stretching and bending vibrations of various bonds are observed in the composite. The phosphate and carbonate bonds for the nHA are also present along with ZnO bond. The peak at 1455 cm⁻¹ showed the asymmetric stretching of CO₃²⁻ while the peak around 878.2 cm⁻¹ in the range of CO₃²⁻ bending vibration. The peak observed around 1047 cm⁻¹ is within the range of asymmetric stretching of PO₄³⁻. The peak around 649.3 cm⁻¹ is within the range of ZnO stretch. No extra peak was observed indicating that no other reaction took place.

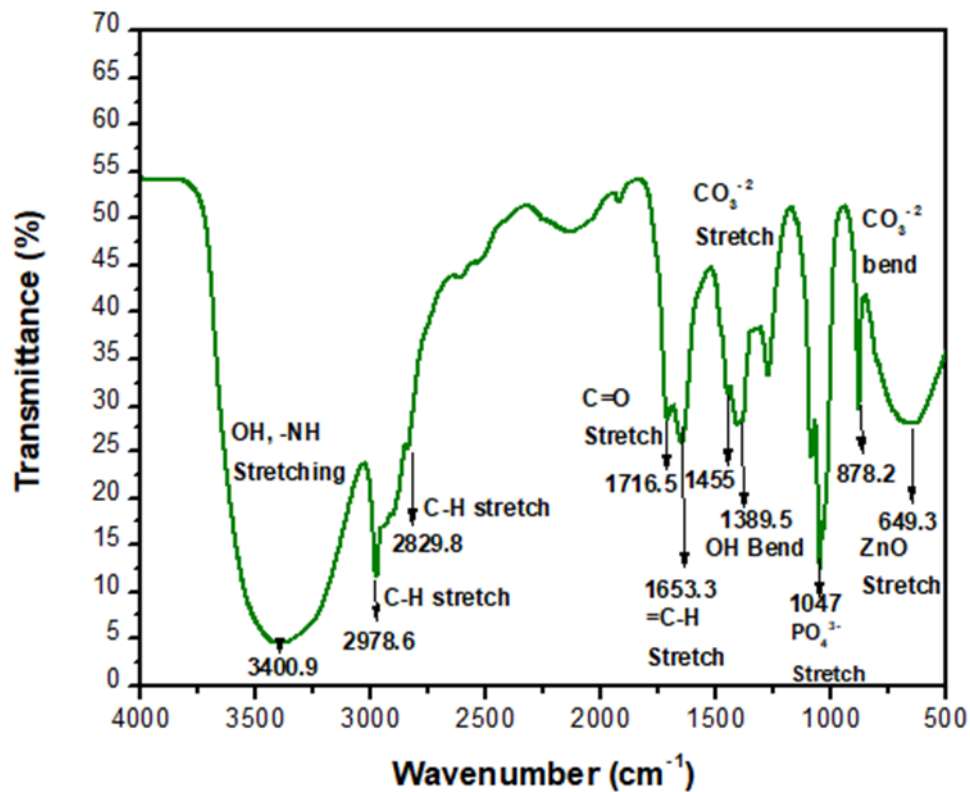


Figure 11: FTIR of Ch/ nHA/ ZnO

5.3 Scanning Electron Microscopy (SEM)

SEM analysis was used for the morphology and crystal structure analysis of our prepared samples. SEM was performed at SCME, NUST. The SEM analysis of our samples is as follows:

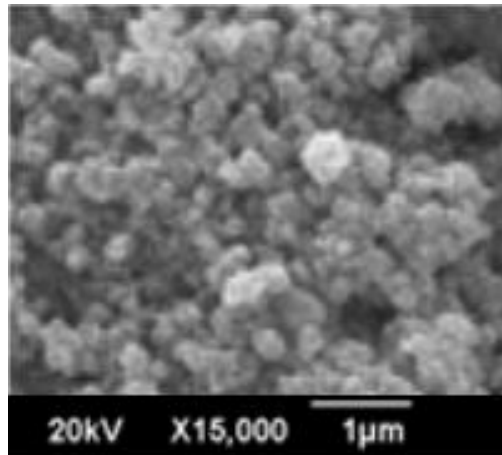


Figure 12: SEM of Chitosan

The SEM image shows the Chitosan nanoparticles we purchased from Sigma Aldrich. The size of the nanoparticles was in submicrons.

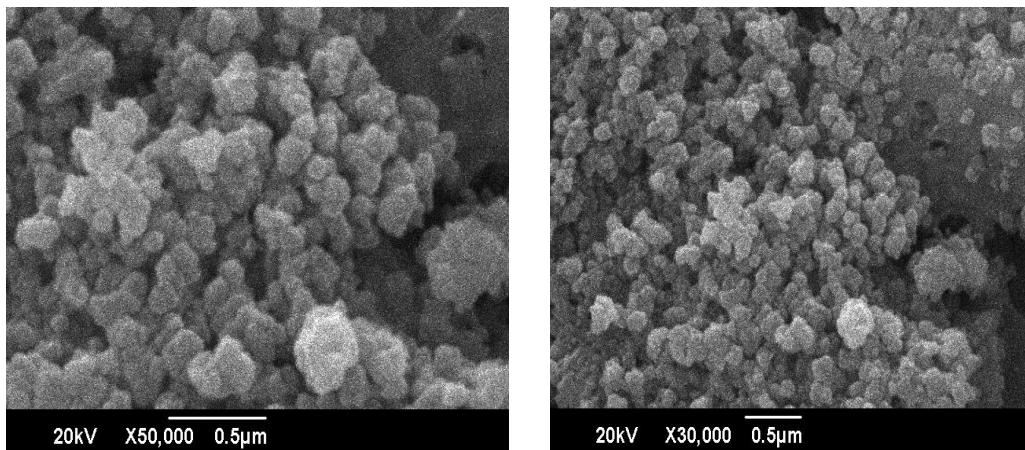


Figure 13: SEM of ZnO NP

The ZnO nanoparticles were synthesized by co-precipitation method. Zinc Nitrate and Sodium Hydroxide as precursors. Acetic acid was used as a capping agent. The resulting nanoparticles are highly aggregated having a rough surface. The particles have hexagonal wurtzite structure having a particle size in submicrons.

In the hexagonal wurtzite structure, O^{2-} ions are situated in the hexagonal close packing (hcp) arrangement of lattice sites, while Zn^{2+} ions position themselves in alternate tetrahedral holes. This is in contrast to the zinc blende structure, where O^{2-} ions form a cubic close packing (ccp) array, and Zn^{2+} ions occupy tetrahedral voids [97].

According to a recent study, agglomeration of ZnO nanoparticles can occur during synthesis using the co-precipitation method [98].

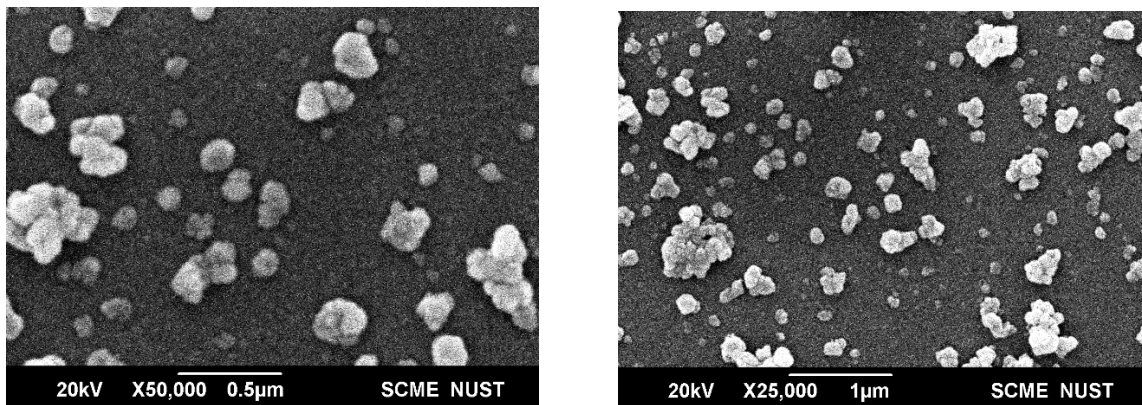


Figure 14: SEM of nHA

Hydroxyapatite nanoparticles (HANPs) are synthesized by wet chemical precipitation method. The materials used were calcium nitrate tetrahydrate [$Ca(NO_3)_2 \cdot 4H_2O$] and di-ammonium hydrogen phosphate $(NH_4)_2 HPO_4$. The morphology analysis revealed the clustering of spherical hydroxyapatite particles (HAPs), with an average nanoparticle size of approximately 34.95 nanometers [93, 99].

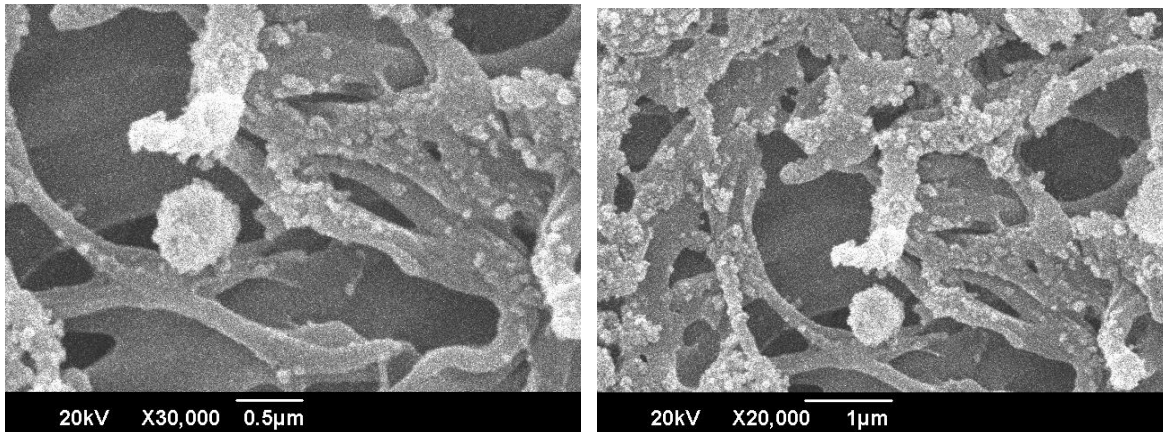


Figure 15: SEM of Ch/ nHA/ZnO

The SEM analysis of our composite material showed an amorphous matrix with nanoparticles embedded inside. It shows a porous structure with nanoparticles embedded inside. Nanohydroxyapatite and zinc oxide fillers embed within a chitosan matrix.

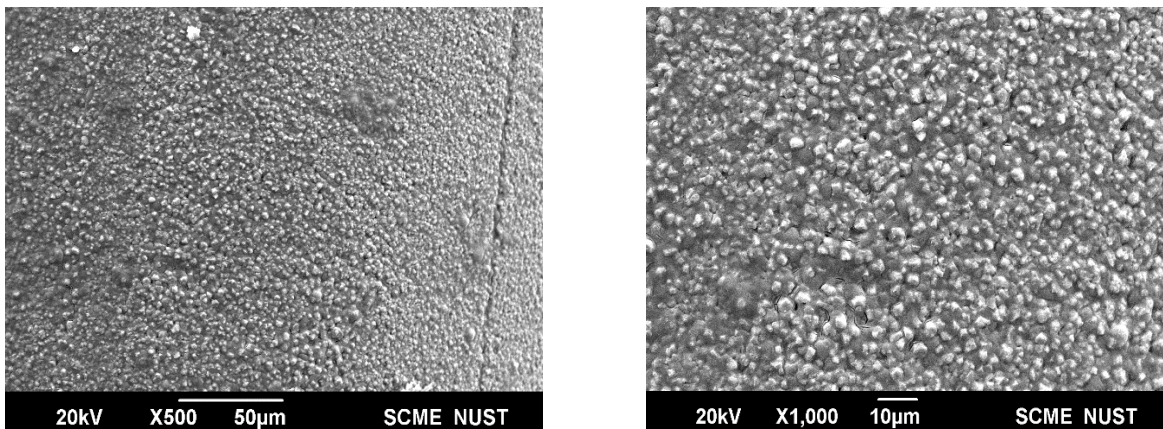


Figure 16: SEM of ZnO coated on SSP

The analysis of the SSPs coated with ZnO showed that these nanoparticles are coated or deposited in the form of sheets. The sheets are not uniform as the particles feel like somehow suspended. As per a research article published in the Archives of Civil and Mechanical Engineering, investigations have been conducted on the suitability of atomic layer deposited ZnO films on stainless steel for biomedical applications. [100, 101].

The study also tested the corrosion resistance of the ZnO layer on the substrate made of 316 LVM steel and found that it had a beneficial effect on the substrate [100, 101].

The hydroxyapatite is not in the form of sheets but as suspended nanoparticles in a liquid medium. This method allows for the precise deposition of HA onto stainless steel surfaces, enabling the creation of coatings with desired properties and thickness for various applications, such as biomedical implants or corrosion resistance.

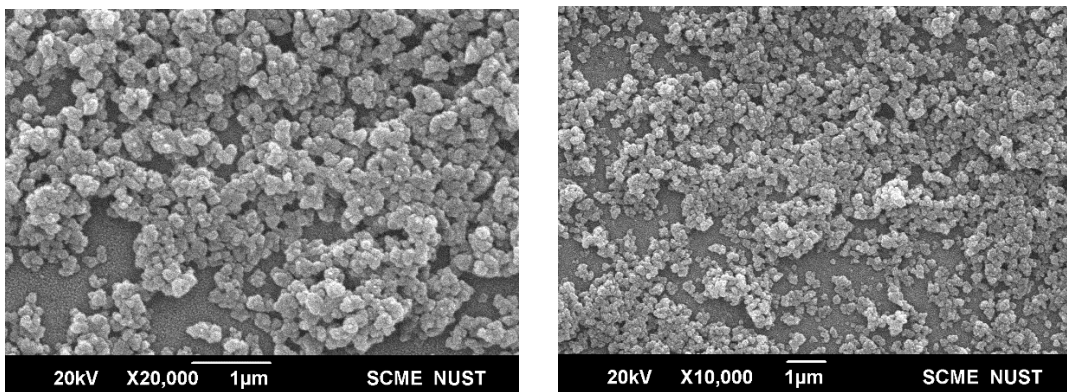


Figure 17: SEM of nHA on SSP

SEM images of HAP-coated substrates reveal cauliflower-like structures on the surface. Additionally, the HAP coatings formed do not provide complete coverage of the substrate surface. [102].

Electrophoretic deposition (EPD) was used to deposit charged particles onto a substrate. Hydroxyapatite (HA) coatings can be deposited on stainless steel substrates using the EPD method. The HA coatings can be used to improve the biocompatibility of stainless-steel implants.

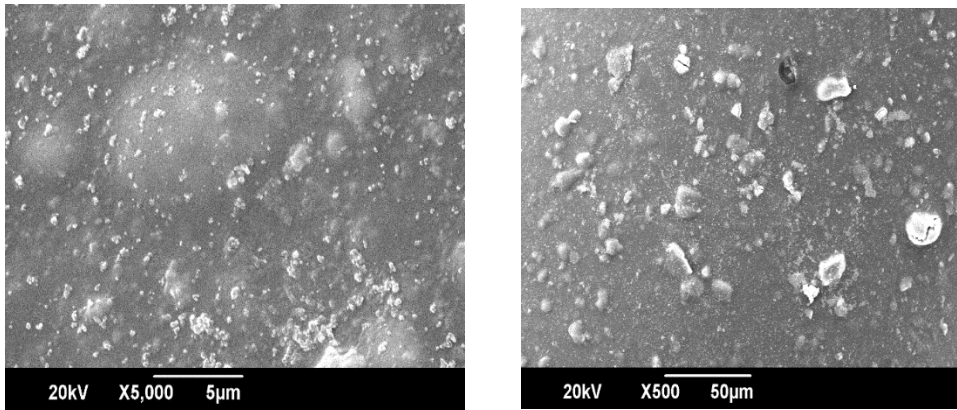


Figure 18: SEM of Ch/ nHA/ ZnO coated on SSP

The SEM analysis showed our composite is coated in a form of thin layer on stainless steel pins. It is a thin layer nano- scale coating containing chitosan as a matrix with nHA and ZnO NPs embedded inside. The SEM image showed a thin film formation over our SSPs substrate. The coatings exhibited uniformity, and the image revealed no segregation of particles at any point. [103].

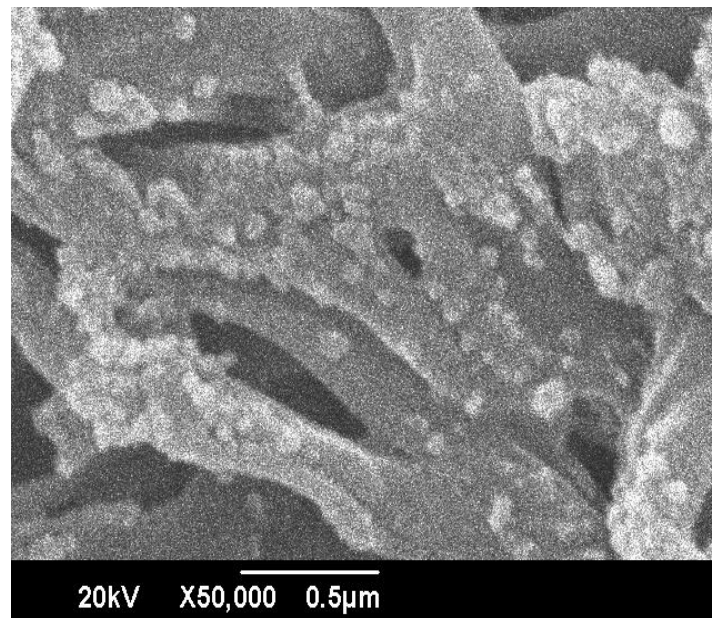


Figure 19: SEM of Ch/ nHA/ ZnO coated on SSP (closer view)

This image shows the closed image of our coating. This shows what is inside the film. The observation of a flower-like structure and cluster morphology indicates the effective mixing and presence of nHA and ZnO NPs in the coating [103]. Within the film, a notable flower-like structure and clustered morphology are discernible, signifying the proper integration of nanoscale hydroxyapatite (nHA) and zinc oxide nanoparticles (ZnO NPs) within the porous coating. This observation further reinforces the presence of coalescence in certain areas of the composites, a phenomenon commonly observed in natural polymer composites where voids tend to be filled with complementary components.

5.4 Electrochemical corrosion in Hank's Solution

Hank's solution was used as an electrolyte for our case. It was prepared according to the method mentioned before. Our working electrode was the surgical staple pin (coated and uncoated), the reference electrode was Ag/AgCl while platinum wire was used as auxiliary electrode or counter electrode. First the stability of the solution was checked [104].

The working electrode was dipped into the electrolyte for 30 mins to stabilize the circuit potential. The Potential window was set between (-1.6 to 0.2) V. The electrodes were dipped into electrolyte and the test was performed using our different samples as working electrode one by one. The samples include uncoated stainless-steel pin (SSP), SSP coated with chitosan, SSP coated with ZnO Oxide nanoparticles (coated in the form of sheets after analyzing in SEM), SSP coated with nanohydroxyapatite, and SSP coated with the composite of three meaning Ch /nHA/ ZnO Composite.

The table 1 indicates that corrosion potential is increasing negatively in case of coatings as compared to the bare sample, while there is a considerable decrease in the I_{corr} values. This means more potential is required for corrosion to start as indicated by E_{corr} values and once the corrosion starts the corrosion rate is slow as indicated by the decreasing I_{corr} values.

The results demonstrate that the corrosion resistance of the substrate is enhanced with the coated materials. The corrosion rate exhibits a direct correlation with the values of I_{corr} , with a noticeable reduction in the corrosion rate accompanying a decrease in I_{corr} values, in

accordance with Faraday's Law. According to this law, rate of corrosion is directly related to the I_{corr} values.

The findings unequivocally establish that the application of our selected materials as coatings on the substrate results in a decrease in the corrosion rate.

The corrosion rate in all instances of coating application exhibits a notable reduction, with particular significance observed in the case of our Ch/ nHA/ ZnO composite when compared to the uncoated (Bare) sample.

The improved corrosion resistance can be attributed to the protective barrier created by these coatings when applied to stainless steel. This barrier effectively mitigates the corrosion rate of the underlying metal by shielding it from direct contact with corrosive agents, such as moisture, chemicals, and salts.

The results clearly indicated that corrosion rate is decreased if any of our selected materials is coated over the substrate.

The increasing order of I_{corr} values is as follows:

Bare > Zinc Coated > Chitosan Coated > nHA Coated > Ch/ nHA/ ZnO Coated.

The corrosion resistance is improved with coating. Corrosion rates in any case of coating have decreased especially with our composite Ch/ nHA/ ZnO compared to Bare Sample. The reason for the improvement is that when coatings are applied over stainless steel, they create a protective barrier that reduces the corrosion rate of the underlying metal.

Here are the plotted results for all the 5 samples,

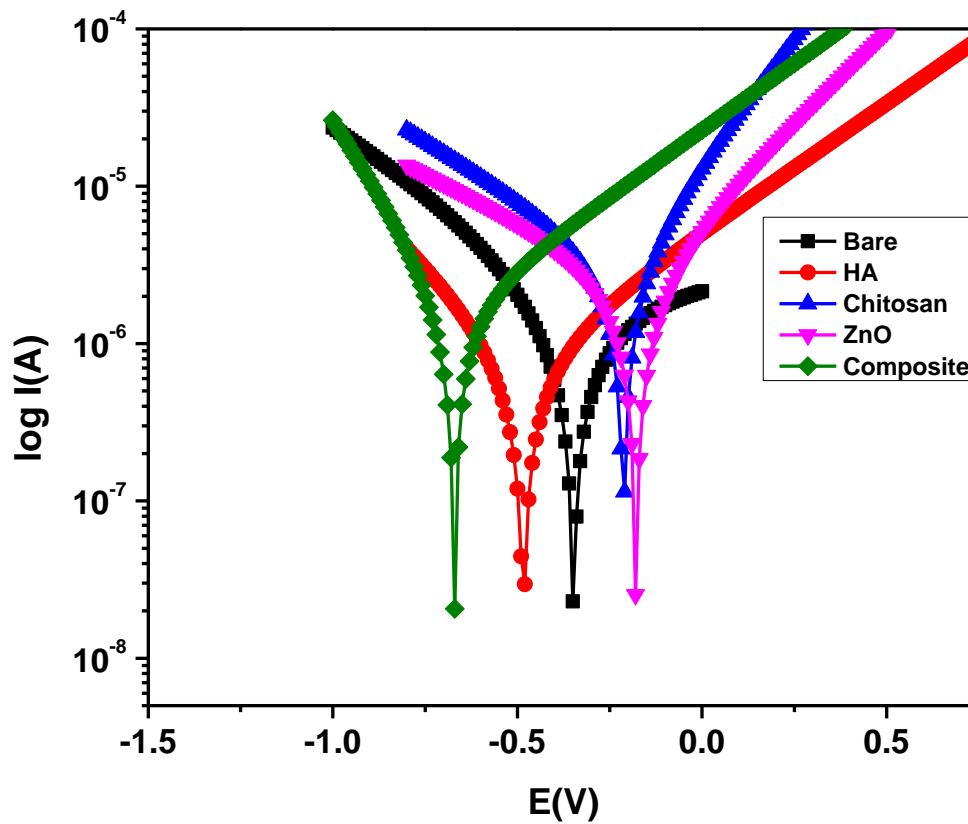


Figure 20: Corrosion Testing Results

The results were analyzed and E_{corr} , I_{corr} , and Corrosion rate (mpy) were calculated.

Table 1: Comparison of the Corrosion Properties

Samples	I_{corr}	E_{corr}	Corr. Rate (mpy)
Bare	3.160 μ A	-3.480 mV	812.6
Chitosan coated	2.630 μ A	-179.0 mV	676.9

ZnO coated	3.140 μ A	-192.0 mV	807.2
nHA coated	2.070 μ A	-213.0 mV	532.0
Ch /nHA /ZnO coated	1.040 μ A	-671.0 mV	266.5

The table above indicated that corrosion potential is increasing negatively in case of coatings as compared to the bare sample, while there is a considerable decrease in the I_{corr} values. This means more potential is required for corrosion to start as indicated by E_{corr} values and once the corrosion starts the corrosion rate is slow as indicated by the decreasing I_{corr} values.

The results demonstrate that the corrosion resistance of the substrate is enhanced with the coated materials. The corrosion rate exhibits a direct correlation with the values of I_{corr} , with a noticeable reduction in the corrosion rate accompanying a decrease in I_{corr} values, in accordance with Faraday's Law. According to this law, rate of corrosion is directly related to the I_{corr} values.

These coatings act as a shield, preventing direct contact between the stainless steel and corrosive elements such as moisture, chemicals, and salts. The coatings on stainless steel substrates are proved effective in the prevention of corrosion and to increase the values of polarization resistance compared to uncoated samples [102].

If we closely observe, the corrosion rate of bare SSPs was to be found as 812.6 mpy and the coatings over it reduced its corrosion rate to a significant value. The decreasing corrosion rate is:

Ch/ nHA/ ZnO Coated < nHA Coated < Chitosan Coated < Zinc Coated < Bare

This indicates that the bare sample is more susceptible to corrosion as compared to other coated samples. In our case the Ch /nHA/ ZnO Composite is comparatively good against corrosion,

or we can say that it has good corrosion resistance against body fluids, we used hank's solution in our case. The coating may survive until the injury is healed; because of the high protection it offers against corrosion [103, 105].

When a coating is applied to a metal surface, it can affect the formation of the chromium oxide layer and the passivation process. This layer is formed on the surface metals that contain chromium. This layer is responsible for providing corrosion resistance to the metal [106, 107].

Passivation is a process that involves creating a protective layer on the surface of a metal to prevent corrosion. The passivation process can be affected by coatings, which can either enhance or reduce the effectiveness of the passivation layer [108].

Upon the application of a coating to a metal surface, it has the capacity to influence both the cathodic and anodic branches of the Tafel plot. The cathodic branch illustrates the reduction reaction taking place at the metal surface, while the anodic branch elucidates the oxidation reaction occurring at the metal surface. [109].

The effect of coatings on the Tafel plot depends on the type of coating and its properties. Some coatings can shift both branches of the Tafel plot to the right, which indicates that they increase the overpotential required for a given current density. This shift indicates that the coating has increased the activation energy for both reactions, which slows down both reaction rates and reduces corrosion 3. Other coatings can shift only one branch of the Tafel plot, which indicates that they affect only one of the electrochemical reactions.

In summary, when a coating is applied to a metal surface, it can affect both the formation of the chromium oxide layer and the passivation process. The effect of coatings on corrosion depends on their properties and their effect on both branches of the Tafel plot.

5.5 Antimicrobial activity

Two tests were performed to check the antimicrobial activity for our powder material and also the coated material against the bacterial strains of *Escherichia coli* and *Staphylococcus aureus*.

For our powder material disc diffusion method was used, and for our coated SSPs Colony Forming Unit (CFU) was used.

5.5.1 Disc Diffusion Method

All the Lab ware to be used was autoclaved first. The bacterial strains were refreshed on Luria agar (L-agar) and were incubated for 24hrs. Already prepared Muller Hinton Agar (MHA) was poured over the petri dishes and was left for solidification.

The inoculum of bacterial strains was spread over petri dishes. 16mg/ml, 20mg/ml, 24mg/ml and 28mg/ml dilutions of our Ch /nHA/ ZnO Composite powder in deionized water were prepared. The filter paper was dipped in our prepared dilution and was placed over the prepared petri dishes. The plates were then placed in incubator for 24hrs.the next day plates were observed.

The composite powder showed maximum antibacterial activity at 24mg/ml and 28mg/ml for both bacterial strains. The inhibition zone calculated against Escherichia coli was approximately 15.3 mm and that against Staphylococcus aureus was approximately 17.3 mm.

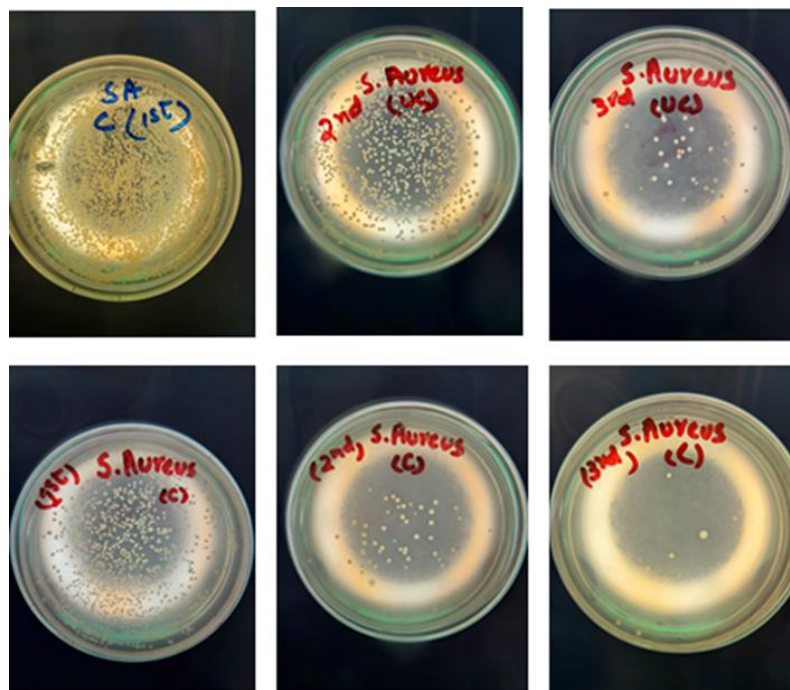
The figures below show the inhibition zones for powdered samples against E. coli and S. aureus.



Figure 21: Incubation zones for against E. coli and S. aureus.

5.5.2 Colony Forming Unit (CFU)

All the Lab ware to be used was autoclaved first. The bacterial strains were refreshed on Luria agar (L-agar) and were incubated for 24hrs. The next day the inoculum of both species was taken and added to separate falcon tubes having PBS solution. The tubes were vortexed. After that the ODI was checked. A total of four tubes were prepared, two for each bacterium (for treated and untreated samples). SSPs were immersed in the tubes and incubated for 24 hrs. The next day, the already prepared Muller Hinton Agar (MHA) was poured over the petri dishes and was left for solidification. Dilutions were prepared from the incubated tubes according to a specific method [72, 110-112]. A total of 20 dilutions were prepared, five for each case. 0.1 ml of each dilution was taken and spread over the petri plates. The plates were incubated, and the colonial growth was checked after 24 hrs.



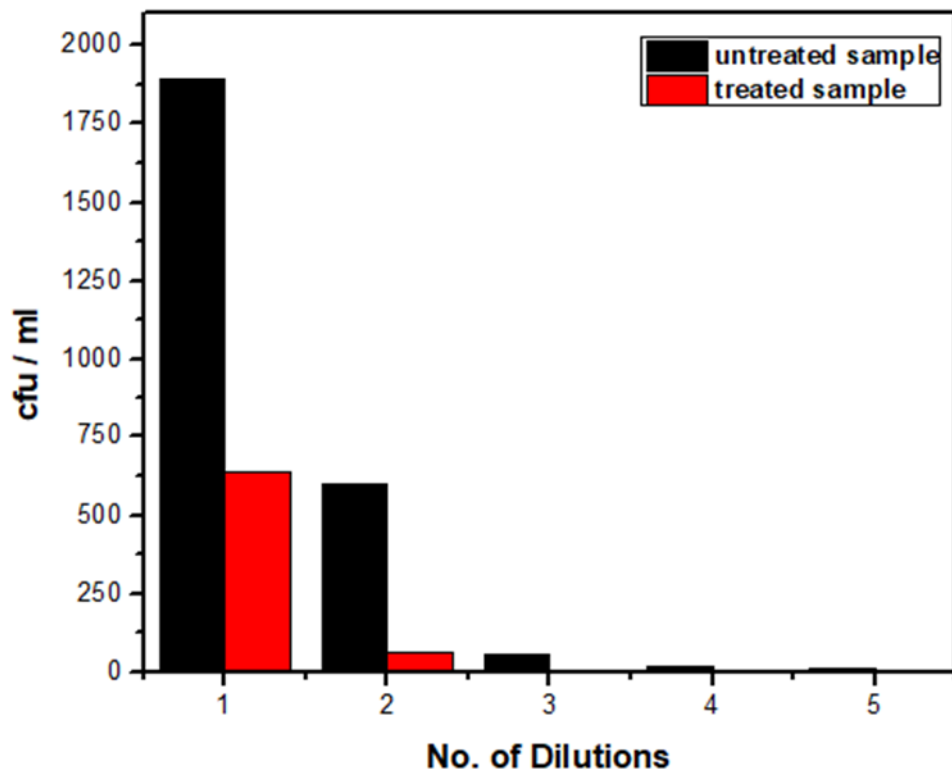


Figure 26: Colonies Growth for treated and untreated *S. aureus* plates

The graph in Fig 26 shows the colonies growth of *Staphylococcus aureus* against our treated and untreated meaning coated and uncoated SSPs. The graph clearly indicates that the cfu/ml for our coated SSPs dropped to a very smaller value as compared to the uncoated SSPs. The drop was clearly observed at second dilution. This is due to the introduction of Zn⁺² ions, having antibacterial properties, from the coating which inhibited the growth of bacteria. The cfu/ml calculated for this dilution was 62×10^3 for coated samples and 600×10^3 for uncoated samples. Similarly in case of third dilution, the cfu/ml values for coated and uncoated samples are 10×10^4 and 57×10^4 respectively.

The colonies for first dilution were uncountable for uncoated material while that for coated were comparatively low. This clearly indicated that our coated or treated sample inhibits the colonial growth of *Staphylococcus aureus*.

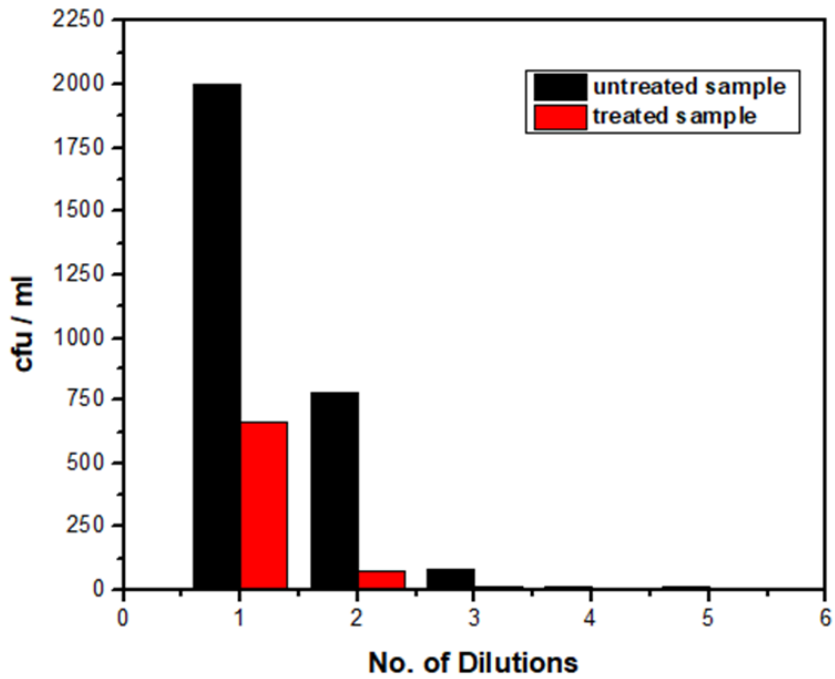
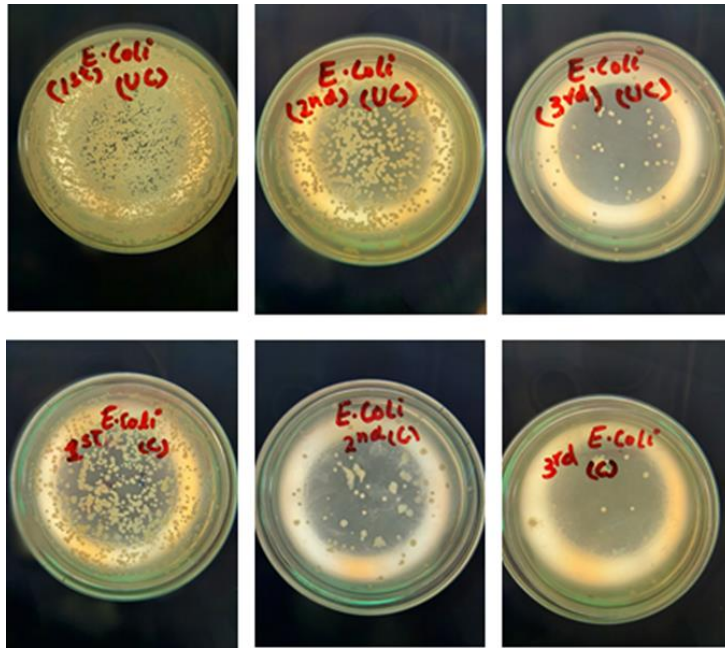


Figure 27: Colonies Growth for treated and untreated E. coli plates

The graph in Fig 27 shows the colonies growth of *Escherichia coli* against our treated and untreated meaning coated and uncoated SSPs. The graph clearly indicates that the cfu/ml for our coated SSPs dropped to a very smaller value as compared to the uncoated SSPs. This is due to the antimicrobial properties of Zn^{+2} ions, which upon releasing from the coating prohibited the growth of bacteria. The drop was clearly observed at second dilution. The cfu/ml calculated for this dilution was 74×10^3 for coated samples and 780×10^3 for uncoated samples. Similarly in case of third dilution, the cfu/ml values for coated and uncoated samples are 13×10^4 and 83×10^4 respectively.

The colonies for first dilution were uncountable for uncoated material while that for coated were comparatively low. This clearly indicated that our coated or treated sample inhibits the colonial growth of *Escherichia coli*.

Conclusion

The successful synthesis of a Ch/nHA/ZnO nano-composite material, demonstrating promising antibacterial and corrosion resistance properties, was achieved in our study. Surgical staple pins were employed as the substrate, which were effectively coated through the Electrophoretic deposition method. The composite coating applied to the surface of the surgical staple pins (SSPs) exhibited enhanced corrosion resistance as compared to their uncoated SSPs. Smaller Icorr values are indicative of reduced corrosion rates, consistent with Faraday's law, which establishes a direct relationship between corrosion rate and Icorr values, serving as an indicator of instantaneous corrosion rate. The coated SSPs exhibited substantially diminished Icorr values in comparison to the uncoated SSPs, thereby satisfying Faraday's Law. Consequently, the coated samples exhibited a noticeable decrease in the corrosion rate. Furthermore, the coating demonstrated effectiveness in suppressing the growth of *E. coli* and *S. aureus* colonies. Notably, the coated samples displayed fewer colonies of both bacterial species when compared to the uncoated samples. Subsequent evaluation of the antifungal properties of the coating is warranted. It is essential to highlight that the entire experiment was conducted in vitro. For an application-oriented perspective, future research should encompass in vivo testing. The surgical staple pins coated with the Ch/nHA/ZnO composite offer antimicrobial and corrosion resistance properties, which hold potential for improving surgical outcomes and supporting the wound healing process.

References

- [1] N. Al-Harbi *et al.*, "Silica-based bioactive glasses and their applications in hard tissue regeneration: A review," *Pharmaceuticals*, vol. 14, no. 2, p. 75, 2021.
- [2] I. Negut, V. Grumezescu, and A. M. Grumezescu, "Treatment strategies for infected wounds," *Molecules*, vol. 23, no. 9, p. 2392, 2018.
- [3] S. N. Michaleas, K. Laios, A. Charalabopoulos, G. Samonis, M. Karamanou, and S. Michaleas, "Joseph Lister (1827-1912): A Pioneer of Antiseptic Surgery," *Cureus*, vol. 14, no. 12, 2022.
- [4] Z. Cope, "Joseph Lister, 1827-1912," *British Medical Journal*, vol. 2, no. 5543, p. 7, 1967.
- [5] S. Dhivya, V. V. Padma, and E. Santhini, "Wound dressings - a review," (in eng), *Biomedicine (Taipei)*, vol. 5, no. 4, p. 22, Dec 2015.
- [6] E. Polykandriotis, J. Daenicke, A. Bolat, J. Grüner, D. W. Schubert, and R. E. Horch, "Individualized Wound Closure-Mechanical Properties of Suture Materials," (in eng), *J Pers Med*, vol. 12, no. 7, Jun 25 2022.
- [7] T. Tshabalala, A. Ndhala, B. Ncube, H. Abdelgadir, and J. Van Staden, "Potential substitution of the root with the leaf in the use of *Moringa oleifera* for antimicrobial, antidiabetic and antioxidant properties," *South African Journal of Botany*, vol. 129, pp. 106-112, 2020.
- [8] C.-Y. Chin, J. Jalil, P. Y. Ng, and S.-F. Ng, "Development and formulation of *Moringa oleifera* standardised leaf extract film dressing for wound healing application," *Journal of ethnopharmacology*, vol. 212, pp. 188-199, 2018.
- [9] A. D. Gaidry, L. Tremblay, D. Nakayama, and R. C. Ignacio Jr, "The history of surgical staplers: a combination of Hungarian, Russian, and American innovation," *The American Surgeon*, vol. 85, no. 6, pp. 563-566, 2019.
- [10] C. E. Azmat and M. Council, "Wound closure techniques," 2017.
- [11] S. Ghosh, N. More, and G. Kapusetti, "Surgical staples: Current state-of-the-art and future prospective," *Medicine in Novel Technology and Devices*, p. 100166, 2022.
- [12] H. Amano *et al.*, "Biodegradable surgical staple composed of magnesium alloy," *Scientific reports*, vol. 9, no. 1, p. 14671, 2019.

- [13] P. Y. G. Choy, I. P. Bissett, J. G. Docherty, B. R. Parry, A. Merrie, and A. Fitzgerald, "Stapled versus handsewn methods for ileocolic anastomoses," *Cochrane Database of Systematic Reviews*, no. 9, 2011.
- [14] H. Amano *et al.*, "The impact of body weight on stapled anastomosis in pediatric patients," *Journal of Pediatric Surgery*, vol. 53, no. 10, pp. 2036-2040, 2018.
- [15] B. Moran, "Stapling instruments for intestinal anastomosis in colorectal surgery," *British journal of surgery*, vol. 83, no. 7, pp. 902-909, 1996.
- [16] E. Chekan and R. L. Whelan, "Surgical stapling device-tissue interactions: what surgeons need to know to improve patient outcomes," (in eng), *Med Devices (Auckl)*, vol. 7, pp. 305-18, 2014.
- [17] D. Hofmann, M. Entrialgo-Castaño, K. Kratz, and A. Lendlein, "Knowledge-based approach towards hydrolytic degradation of polymer-based biomaterials," *Advanced materials*, vol. 21, no. 32-33, pp. 3237-3245, 2009.
- [18] R. Felfel *et al.*, "In vitro degradation and mechanical properties of PLA-PCL copolymer unit cell scaffolds generated by two-photon polymerization," *Biomedical materials*, vol. 11, no. 1, p. 015011, 2016.
- [19] H. Wu *et al.*, "Research of a novel biodegradable surgical staple made of high purity magnesium," *Bioactive materials*, vol. 1, no. 2, pp. 122-126, 2016.
- [20] F. Witte, "The history of biodegradable magnesium implants: a review," *Acta biomaterialia*, vol. 6, no. 5, pp. 1680-1692, 2010.
- [21] A. Samir, F. H. Ashour, A. A. Hakim, and M. Bassyouni, "Recent advances in biodegradable polymers for sustainable applications," *Npj Materials Degradation*, vol. 6, no. 1, p. 68, 2022.
- [22] S. Demertzis *et al.*, "Beyond the "B": a new concept of the surgical staple enabling miniature staplers," *Surgical Endoscopy*, vol. 29, pp. 3674-3684, 2015.
- [23] J. Nitsche, C. Howell, and T. Howell, "Skin closure with subcuticular absorbable staples after cesarean section is associated with decreased analgesic use," *Archives of gynecology and obstetrics*, vol. 285, pp. 979-983, 2012.
- [24] H. Zhang, J. Han, Y. Sun, Y. Huang, and M. Zhou, "MC3T3-E1 cell response to stainless steel 316L with different surface treatments," *Materials Science and Engineering: C*, vol. 56, pp. 22-29, 2015.
- [25] A. Bekmurzayeva, W. J. Duncanson, H. S. Azevedo, and D. Kanayeva, "Surface modification of stainless steel for biomedical applications: Revisiting a century-old material," *Materials Science and Engineering: C*, vol. 93, pp. 1073-1089, 2018.

- [26] J. Walczak, F. Shahgaldi, and F. Heatley, "In vivo corrosion of 316L stainless-steel hip implants: morphology and elemental compositions of corrosion products," *Biomaterials*, vol. 19, no. 1-3, pp. 229-237, 1998.
- [27] T. Roland, D. Reirant, K. Lu, and J. Lu, "Fatigue life improvement through surface nanostructuring of stainless steel by means of surface mechanical attrition treatment," *Scripta Materialia*, vol. 54, no. 11, pp. 1949-1954, 2006.
- [28] C.-C. Shih, C.-M. Shih, Y.-Y. Su, L. H. J. Su, M.-S. Chang, and S.-J. Lin, "Effect of surface oxide properties on corrosion resistance of 316L stainless steel for biomedical applications," *Corrosion Science*, vol. 46, no. 2, pp. 427-441, 2004.
- [29] S. Virtanen, I. Milošev, E. Gomez-Barrena, R. Trebše, J. Salo, and Y. T. Kontinen, "Special modes of corrosion under physiological and simulated physiological conditions," *Acta biomaterialia*, vol. 4, no. 3, pp. 468-476, 2008.
- [30] Q. Chen and G. A. Thouas, "Metallic implant biomaterials," *Materials Science and Engineering: R: Reports*, vol. 87, pp. 1-57, 2015.
- [31] E. Medilanski, K. Kaufmann, L. Y. Wick, O. Wanner, and H. Harms, "Influence of the surface topography of stainless steel on bacterial adhesion," *Biofouling*, vol. 18, no. 3, pp. 193-203, 2002.
- [32] B. Seo, H. Kanematsu, M. Nakamoto, Y. Miyabayashi, M. Suzuki, and T. Tanaka, "Corrosion and antibacterial performance of 316L stainless steel with copper patterns by super-spread wetting of liquid copper," *Surface and Coatings Technology*, vol. 462, p. 129496, 2023.
- [33] E. K. Bliven, M. Greinwald, S. Hackl, and P. Augat, "External fixation of the lower extremities: Biomechanical perspective and recent innovations," *Injury*, vol. 50, pp. S10-S17, 2019.
- [34] A. Saithna, "The influence of hydroxyapatite coating of external fixator pins on pin loosening and pin track infection: a systematic review," *Injury*, vol. 41, no. 2, pp. 128-132, 2010.
- [35] C. R. Arciola, L. Montanaro, A. Moroni, M. Giordano, A. Pizzoferrato, and M. E. Donati, "Hydroxyapatite-coated orthopaedic screws as infection resistant materials: in vitro study," *Biomaterials*, vol. 20, no. 4, pp. 323-327, 1999.
- [36] J. G. Lane, R. A. Sachs, and B. Riehl, "Arthroscopic staple capsulorrhaphy: a long-term follow-up," *Arthroscopy: The Journal of Arthroscopic & Related Surgery*, vol. 9, no. 2, pp. 190-194, 1993.

- [37] K. Y. Lee, L. Jeong, Y. O. Kang, S. J. Lee, and W. H. Park, "Electrospinning of polysaccharides for regenerative medicine," *Advanced drug delivery reviews*, vol. 61, no. 12, pp. 1020-1032, 2009.
- [38] H. M. Ibrahim and E. M. R. E.-. Zairy, "Chitosan as a Biomaterial — Structure, Properties, and Electrospun Nanofibers," in *Concepts, Compounds and the Alternatives of Antibacterials*, B. Varaprasad, Ed. Rijeka: IntechOpen, 2015, p. Ch. 4.
- [39] J. Yang, F. Tian, Z. Wang, Q. Wang, Y. J. Zeng, and S. Q. Chen, "Effect of chitosan molecular weight and deacetylation degree on hemostasis," *Journal of Biomedical Materials Research Part B: Applied Biomaterials*, vol. 84, no. 1, pp. 131-137, 2008.
- [40] I. Wedmore, J. G. McManus, A. E. Pusateri, and J. B. Holcomb, "A special report on the chitosan-based hemostatic dressing: experience in current combat operations," *Journal of Trauma and Acute Care Surgery*, vol. 60, no. 3, pp. 655-658, 2006.
- [41] S. Şenel and S. J. McClure, "Potential applications of chitosan in veterinary medicine," *Advanced drug delivery reviews*, vol. 56, no. 10, pp. 1467-1480, 2004.
- [42] M. Alaei, M. Atapour, and S. Labbaf, "Electrophoretic deposition of chitosan-bioactive glass nanocomposite coatings on AZ91 Mg alloy for biomedical applications," *Progress in Organic Coatings*, vol. 147, p. 105803, 2020.
- [43] S. Heise *et al.*, "Electrophoretic deposition and characterization of chitosan/bioactive glass composite coatings on Mg alloy substrates," *Electrochimica Acta*, vol. 232, pp. 456-464, 2017.
- [44] I. Negut and C. Ristoscu, "Bioactive Glasses for Soft and Hard Tissue Healing Applications—A Short Review," *Applied Sciences*, vol. 13, no. 10, p. 6151, 2023.
- [45] J. Larouche, S. Sheoran, K. Maruyama, and M. M. Martino, "Immune regulation of skin wound healing: mechanisms and novel therapeutic targets," *Advances in wound care*, vol. 7, no. 7, pp. 209-231, 2018.
- [46] T. A. Ostomel, Q. Shi, C. K. Tsung, H. Liang, and G. D. Stucky, "Spherical bioactive glass with enhanced rates of hydroxyapatite deposition and hemostatic activity," *Small*, vol. 2, no. 11, pp. 1261-1265, 2006.
- [47] H. N. Wilkinson, S. Iveson, P. Catherall, and M. J. Hardman, "A novel silver bioactive glass elicits antimicrobial efficacy against *Pseudomonas aeruginosa* and *Staphylococcus aureus* in an ex vivo skin wound biofilm model," *Frontiers in Microbiology*, vol. 9, p. 1450, 2018.

- [48] J. Li *et al.*, "Preparation of copper-containing bioactive glass/eggshell membrane nanocomposites for improving angiogenesis, antibacterial activity and wound healing," *Acta biomaterialia*, vol. 36, pp. 254-266, 2016.
- [49] X. Dong, J. Chang, and H. Li, "Bioglass promotes wound healing through modulating the paracrine effects between macrophages and repairing cells," *Journal of Materials Chemistry B*, vol. 5, no. 26, pp. 5240-5250, 2017.
- [50] Y. Xu, C. Chen, P. B. Hellwarth, and X. Bao, "Biomaterials for stem cell engineering and biomanufacturing," (in eng), *Bioact Mater*; vol. 4, pp. 366-379, Dec 2019.
- [51] M. P. Lutolf, P. M. Gilbert, and H. M. Blau, "Designing materials to direct stem-cell fate," *Nature*, vol. 462, no. 7272, pp. 433-441, 2009.
- [52] N. Ribeiro *et al.*, "New prospects in skin regeneration and repair using nanophased hydroxyapatite embedded in collagen nanofibers," (in eng), *Nanomedicine*, vol. 33, p. 102353, Apr 2021.
- [53] X.-J. Ji *et al.*, "Corrosion resistance and antibacterial properties of hydroxyapatite coating induced by gentamicin-loaded polymeric multilayers on magnesium alloys," *Colloids and Surfaces B: Biointerfaces*, vol. 179, pp. 429-436, 2019.
- [54] J. Kolmas, E. Groszyk, and D. Kwiatkowska-Różycka, "Substituted Hydroxyapatites with Antibacterial Properties," *BioMed Research International*, vol. 2014, p. 178123, 2014/05/11 2014.
- [55] A. Keyvani, M. Zamani, M. Bahamirian, E. Nikoomanzari, A. Fattah-Alhosseini, and H. Sina, "Role of incorporation of ZnO nanoparticles on corrosion behavior of ceramic coatings developed on AZ31 magnesium alloy by plasma electrolytic oxidation technique," *Surfaces and Interfaces*, vol. 22, p. 100728, 2021.
- [56] M. Martínez-Carmona, Y. Gun'ko, and M. Vallet-Regí, "ZnO Nanostructures for Drug Delivery and Theranostic Applications," *Nanomaterials*, vol. 8, no. 4, p. 268, 2018.
- [57] D. Liu *et al.*, "Surface functionalization of ZnO nanotetrapods with photoactive and electroactive organic monolayers," *Langmuir*, vol. 24, no. 9, pp. 5052-5059, 2008.
- [58] O. Taratula *et al.*, "Binding studies of molecular linkers to ZnO and MgZnO nanotip films," *The Journal of Physical Chemistry B*, vol. 110, no. 13, pp. 6506-6515, 2006.
- [59] M. Chhowalla, H. S. Shin, G. Eda, L.-J. Li, K. P. Loh, and H. Zhang, "The chemistry of two-dimensional layered transition metal dichalcogenide nanosheets," *Nature chemistry*, vol. 5, no. 4, pp. 263-275, 2013.

- [60] B. Fotovvati, N. Namdari, and A. Dehghanghadikolaei, "On Coating Techniques for Surface Protection: A Review," *Journal of Manufacturing and Materials Processing*, vol. 3, no. 1, p. 28, 2019.
- [61] M. Khalid, M. Mujahid, S. Amin, R. Rawat, A. Nusair, and G. Deen, "Effect of surfactant and heat treatment on morphology, surface area and crystallinity in hydroxyapatite nanocrystals," *Ceramics International*, vol. 39, no. 1, pp. 39-50, 2013.
- [62] P. Bindra, H. Gerischer, and D. Kolb, "Electrolytic deposition of thin metal films on semiconductor substrates," *Journal of the Electrochemical Society*, vol. 124, no. 7, p. 1012, 1977.
- [63] L. Zhang, H. Sun, J. Yu, H. Yang, F. Song, and C. Huang, "Application of electrophoretic deposition to occlude dentinal tubules in vitro," *Journal of Dentistry*, vol. 71, pp. 43-48, 2018.
- [64] A. R. Boccaccini, J. Cho, J. A. Roether, B. J. Thomas, E. J. Minay, and M. S. Shaffer, "Electrophoretic deposition of carbon nanotubes," *Carbon*, vol. 44, no. 15, pp. 3149-3160, 2006.
- [65] J. H. Dickerson and A. R. Boccaccini, *Electrophoretic deposition of nanomaterials*. Springer, 2011.
- [66] A. J. Ahamed and P. V. Kumar, "Synthesis and characterization of ZnO nanoparticles by co-precipitation method at room temperature," *Journal of Chemical and Pharmaceutical Research*, vol. 8, no. 5, pp. 624-628, 2016.
- [67] M. Abd Mutalib, M. Rahman, M. Othman, A. Ismail, and J. Jaafar, "Scanning electron microscopy (SEM) and energy-dispersive X-ray (EDX) spectroscopy," in *Membrane characterization*: Elsevier, 2017, pp. 161-179.
- [68] D. C. Joy and J. B. Pawley, "High-resolution scanning electron microscopy," *Ultramicroscopy*, vol. 47, no. 1-3, pp. 80-100, 1992.
- [69] L. Laperrière and G. Reinhart, *CIRP encyclopedia of production engineering*. Springer Berlin, 2014.
- [70] J. P. Painuly, "Barriers to renewable energy penetration; a framework for analysis," *Renewable energy*, vol. 24, no. 1, pp. 73-89, 2001.
- [71] C. Berthomieu and R. Hienerwadel, "Fourier transform infrared (FTIR) spectroscopy," *Photosynthesis research*, vol. 101, pp. 157-170, 2009.
- [72] M. Balouiri, M. Sadiki, and S. K. Ibsouda, "Methods for in vitro evaluating antimicrobial activity: A review," (in eng), *J Pharm Anal*, vol. 6, no. 2, pp. 71-79, Apr 2016.

- [73] N. Heatley, "A method for the assay of penicillin," *Biochemical Journal*, vol. 38, no. 1, p. 61, 1944.
- [74] R. Humphries, A. M. Bobenchik, J. A. Hindler, and A. N. Schuetz, "Overview of changes to the clinical and laboratory standards institute performance standards for antimicrobial susceptibility testing, M100," *Journal of clinical microbiology*, vol. 59, no. 12, pp. 10.1128/jcm. 00213-21, 2021.
- [75] M. A. Pfaller, D. J. Sheehan, and J. H. Rex, "Determination of fungicidal activities against yeasts and molds: lessons learned from bactericidal testing and the need for standardization," (in eng), *Clin Microbiol Rev*, vol. 17, no. 2, pp. 268-80, Apr 2004.
- [76] A. Fattah-alhosseini, M. Molaei, M. Nouri, and K. Babaei, "Antibacterial activity of bioceramic coatings on Mg and its alloys created by plasma electrolytic oxidation (PEO): A review," *Journal of Magnesium and Alloys*, vol. 10, no. 1, pp. 81-96, 2022/01/01/ 2022.
- [77] J. Reynolds, "Serial dilution protocols," *American Society for Microbiology: Washington, DC, USA*, pp. 1-7, 2005.
- [78] N. A. Scilletta, M. Pezzoni, M. F. Desimone, G. Soler-Illia, M. G. Bellino, and P. N. Catalano, "Determination of Antibacterial Activity of Film Coatings Against Four Clinically Relevant Bacterial Strains," (in eng), *Bio Protoc*, vol. 11, no. 2, p. e3887, Jan 20 2021.
- [79] D. d. S. Biron, V. d. Santos, and C. P. Bergmann, "Synthesis and characterization of zinc oxide obtained by combining zinc nitrate with sodium hydroxide in polyol medium," *Materials Research*, vol. 23, p. e20200080, 2020.
- [80] R. Panda, M. Hsieh, R. Chung, and T. Chin, "FTIR, XRD, SEM and solid state NMR investigations of carbonate-containing hydroxyapatite nano-particles synthesized by hydroxide-gel technique," *Journal of Physics and Chemistry of Solids*, vol. 64, no. 2, pp. 193-199, 2003.
- [81] A. Fatoni, P. L. Hariani, H. Hermansyah, and A. Lesbani, "Synthesis and characterization of chitosan linked by methylene bridge and schiff base of 4, 4-diaminodiphenyl ether-vanillin," *Indonesian Journal of Chemistry*, vol. 18, no. 1, pp. 92-101, 2018.
- [82] N. Li and R. Bai, "A novel amine-shielded surface cross-linking of chitosan hydrogel beads for enhanced metal adsorption performance," *Industrial & engineering chemistry research*, vol. 44, no. 17, pp. 6692-6700, 2005.
- [83] J. Wang and H. Wang, "Preparation of soluble p-aminobenzoyl chitosan ester by Schiff's base and antibacterial activity of the derivatives," *International journal of biological macromolecules*, vol. 48, no. 3, pp. 523-529, 2011.

- [84] S. Yasmeen, M. Kabiraz, B. Saha, M. Qadir, M. Gafur, and S. Masum, "Chromium (VI) ions removal from tannery effluent using chitosan-microcrystalline cellulose composite as adsorbent," *International Research Journal of Pure and Applied Chemistry*, vol. 10, no. 4, pp. 1-14, 2016.
- [85] K. F. Hasan, H. Wang, S. Mahmud, and C. Genyang, "Coloration of aramid fabric via in-situ biosynthesis of silver nanoparticles with enhanced antibacterial effect," *Inorganic Chemistry Communications*, vol. 119, p. 108115, 2020.
- [86] A. K. Dikshit, P. Banerjee, N. Mukherjee, and P. Chakrabarti, "Theoretical optimization of double dielectric back reflector layer for thin c-Si based advanced solar cells with notable enhancement in MAPD," *Superlattices and Microstructures*, vol. 149, p. 106747, 2021.
- [87] J. A. Delezuk, D. E. Ramírez-Herrera, B. E.-F. de Ávila, and J. Wang, "Chitosan-based water-propelled micromotors with strong antibacterial activity," *Nanoscale*, vol. 9, no. 6, pp. 2195-2200, 2017.
- [88] A. Yadav *et al.*, "Functional finishing in cotton fabrics using zinc oxide nanoparticles," *Bulletin of materials Science*, vol. 29, pp. 641-645, 2006.
- [89] S. M. Costa, D. P. Ferreira, A. Ferreira, F. Vaz, and R. Fangueiro, "Multifunctional flax fibres based on the combined effect of silver and zinc oxide (Ag/ZnO) nanostructures," *Nanomaterials*, vol. 8, no. 12, p. 1069, 2018.
- [90] M. Fiedot-Toboła *et al.*, "Deposition of zinc oxide on different polymer textiles and their antibacterial properties," *Materials*, vol. 11, no. 5, p. 707, 2018.
- [91] R. Pandimurugan and S. Thambidurai, "UV protection and antibacterial properties of seaweed capped ZnO nanoparticles coated cotton fabrics," *International journal of biological macromolecules*, vol. 105, pp. 788-795, 2017.
- [92] A. Chandrasekar, S. Sagadevan, and A. Dakshnamoorthy, "Synthesis and characterization of nano-hydroxyapatite (n-HAP) using the wet chemical technique," *Int. J. Phys. Sci.*, vol. 8, no. 32, pp. 1639-1645, 2013.
- [93] M. A. Khan, Z. Hussain, U. Liaqat, M. A. Liaqat, and M. Zahoor, "Preparation of PBS/PLLA/HAP Composites by the Solution Casting Method: Mechanical Properties and Biocompatibility," (in eng), *Nanomaterials (Basel)*, vol. 10, no. 9, Sep 8 2020.
- [94] B. Cengiz, Y. Gokce, N. Yildiz, Z. Aktas, and A. Calimli, "Synthesis and characterization of hydroxyapatite nanoparticles," *Colloids and Surfaces A: Physicochemical and Engineering Aspects*, vol. 322, no. 1-3, pp. 29-33, 2008.

- [95] D. Choi, K. G. Marra, and P. N. Kumta, "Chemical synthesis of hydroxyapatite/poly (ϵ -caprolactone) composites," *Materials Research Bulletin*, vol. 39, no. 3, pp. 417-432, 2004.
- [96] E. Karamian, M. Abdellahi, and H. Gheisari, "Fluorine-substituted HA reinforced with zircon as a novel nano-biocomposite ceramic: Preparation and characterization," *International Journal of Materials Research*, vol. 106, no. 12, pp. 1285-1290, 2015.
- [97] S. Raha and M. Ahmaruzzaman, "ZnO nanostructured materials and their potential applications: progress, challenges and perspectives," *Nanoscale Advances*, vol. 4, no. 8, pp. 1868-1925, 2022.
- [98] A. u. R. Khan *et al.*, "Exploration of the antibacterial and wound healing potential of a PLGA/silk fibroin based electrospun membrane loaded with zinc oxide nanoparticles," *Journal of Materials Chemistry B*, 10.1039/D0TB02822C vol. 9, no. 5, pp. 1452-1465, 2021.
- [99] S. K. Mohonta, K. H. Maria, S. Rahman, H. Das, and S. M. Hoque, "Synthesis of hydroxyapatite nanoparticle and role of its size in hydroxyapatite/chitosan–gelatin biocomposite for bone grafting," *International Nano Letters*, vol. 11, pp. 381-393, 2021.
- [100] M. Basiaga *et al.*, "Atomic layer deposited ZnO films on stainless steel for biomedical applications," *Archives of Civil and Mechanical Engineering*, vol. 21, no. 1, p. 1, 2020/11/28 2020.
- [101] S. S. Beaini, C. X. Kronawitter, V. P. Carey, and S. S. Mao, "ZnO deposition on metal substrates: Relating fabrication, morphology, and wettability," *Journal of Applied Physics*, vol. 113, no. 18, 2013.
- [102] A. Büyüksağış and N. Çiftçi, "HAP coatings for biomedical applications: biocompatibility and surface protection against corrosion of Ti, Ti6Al4V and AISI 316L SS," *Protection of Metals and Physical Chemistry of Surfaces*, vol. 56, pp. 834-843, 2020.
- [103] W. Akram *et al.*, "Enhancement of Antibacterial Properties, Surface Morphology and In Vitro Bioactivity of Hydroxyapatite-Zinc Oxide Nanocomposite Coating by Electrophoretic Deposition Technique," *Bioengineering*, vol. 10, no. 6, p. 693, 2023.
- [104] A. B. Inc. (2023). *HBSS (Hank's Balanced Salt Solution) Preparation and Recipe*. Available: <https://www.aatbio.com/resources/buffer-preparations-and-recipes/hbss-hanks-balanced-salt-solution>
- [105] S. A. Zuhdi, "Analysis of Mechanical Properties of Biodegradable Implants Material: Pure Zinc and Stainless Steel 316L for Bone External Fixation," Universitas Andalas, 2023.

- [106] M. Z. Khan, M. T. Mehran, R.-H. Song, J.-W. Lee, S.-B. Lee, and T.-H. Lim, "A simplified approach to predict performance degradation of a solid oxide fuel cell anode," *Journal of Power Sources*, vol. 391, pp. 94-105, 2018.
- [107] P. Khadke, T. Tichter, T. Boettcher, F. Muench, W. Ensinger, and C. Roth, "A simple and effective method for the accurate extraction of kinetic parameters using differential Tafel plots," *Scientific reports*, vol. 11, no. 1, p. 8974, 2021.
- [108] A.-R. El-Sayed, H. S. Mohran, and H. M. Abd El-Lateef, "Corrosion study of zinc, nickel, and zinc-nickel alloys in alkaline solutions by Tafel plot and impedance techniques," *Metallurgical and Materials Transactions A*, vol. 43, pp. 619-632, 2012.
- [109] P. Allongue and S. Blonkowski, "Corrosion of III-V compounds; a comparative study of GaAs and InP: Part I. Electrochemical characterization based on Tafel plot measurements," *Journal of electroanalytical chemistry and interfacial electrochemistry*, vol. 316, no. 1-2, pp. 57-77, 1991.
- [110] G. Horváth, T. Bencsik, K. Ács, and B. Kocsis, "Chapter 12 - Sensitivity of ESBL-Producing Gram-Negative Bacteria to Essential Oils, Plant Extracts, and Their Isolated Compounds," in *Antibiotic Resistance*, K. Kon and M. Rai, Eds.: Academic Press, 2016, pp. 239-269.
- [111] J. S. Prusty, "2 - Antifungal discovery from plant sources," in *Phytoconstituents and Antifungals*, A. Kumar, Ed.: Academic Press, 2022, pp. 15-33.
- [112] L. B. Reller, M. Weinstein, J. H. Jorgensen, and M. J. Ferraro, "Antimicrobial susceptibility testing: a review of general principles and contemporary practices," *Clinical infectious diseases*, vol. 49, no. 11, pp. 1749-1755, 2009.